

## RESEARCH ARTICLE

# Nonlinear Boundary Control and Estimation of Distributed States in a Flexible Manipulator

S. Yaqubi | J. Mattila

Department of Automation Technology and Mechanical Engineering, Tampere University, Tampere, Finland

Correspondence: S. Yaqubi ([sadeq.yaqubi@tuni.fi](mailto:sadeq.yaqubi@tuni.fi))

Received: 14 June 2023 | Revised: 21 January 2025 | Accepted: 29 January 2025

Funding: This work was supported by Academy of Finland under the project “Nonlinear PDE-model-based control of flexible manipulators” (Grant No. 355664).

Keywords: flexible robot control | limited data control | PDE control | PDE observer | uncertain system

## ABSTRACT

This paper presents a novel method for partial differential equation (PDE) endpoint control of a flexible manipulator, without using any form of mathematical simplification in PDE-based calculations. It simultaneously addresses the issue of the unavailability of distributed states in an infinite-dimensional flexible dynamic system. This two-fold approach allows for the incorporation of estimated data describing the pose of the flexible manipulator into a model-based PDE control scheme, facilitating convenient stability analysis and model-based control design. This is achieved while maintaining the easily attainable measurement requirements of standard boundary control techniques, which involve the installation of sensors solely at the manipulator's endpoint. To this end, initially a practical, stability-proved distributed state observer is presented which is capable of estimating the deflection of the link throughout the length of the flexible arm based on a nonlinear PDE model. To reduce design complexity and the intensity of implementation, the observation is conducted using a novel partial state observer, which relies on a reduced number of system equations corresponding to the distributed state measurement error. Subsequently, the estimated states are used to construct a boundary controller for state tracking and the elimination of endpoint deflection, resulting in precise endpoint control. Furthermore, inevitable deviations from the nominal model are considered, ensuring the boundedness of the closed-loop system response in the presence of parametric uncertainties through an adaptive design. A rigorous stability analysis of all elements of the closed-loop systems incorporating PDE models is conducted based on Lyapunov stability theory and the extended LaSalle's invariance principle for infinite-dimensional systems. Numerical simulations and analysis demonstrate the precision and efficiency of the proposed solutions.

## 1 | Introduction

### 1.1 | Overview

For decades, a prevailing trend in machine design has been the construction of lighter hardware to achieve higher payload-to-weight ratios, which in turn leads to greater energy efficiency and reduced pollution. This trend has driven the

increasing adoption of flexible robotic systems over their earlier rigid counterparts in a wide range of applications, from aerospace to industrial robotics. However, without well-developed control tools, undesired phenomena such as reduced efficiency and loss of precision due to vibrational effects can impede the adoption of these lightweight, energy-efficient, and flexible robots. These drawbacks counteract the anticipated benefits, and only appropriate automation solutions can unlock their full potential.

This is an open access article under the terms of the [Creative Commons Attribution-NonCommercial-NoDerivs](https://creativecommons.org/licenses/by-nc-nd/4.0/) License, which permits use and distribution in any medium, provided the original work is properly cited, the use is non-commercial and no modifications or adaptations are made.

© 2025 The Author(s). *International Journal of Robust and Nonlinear Control* published by John Wiley & Sons Ltd.

Consequently, the development of sophisticated control schemes tailored to flexible robotic systems has become a significant research focus.

The challenges involved in the precise control of flexible robots differ fundamentally from those of their rigid counterparts. Describing link flexibility mathematically requires expressing it as a collection of distributed states corresponding to the configuration of the flexible links along their length [1, 2]. This is achieved using models in the form of infinite-dimensional partial differential equations (PDEs) and subsequently designing corresponding control schemes for the PDE system. Traditionally, approximations of PDE systems as ordinary differential equations (ODEs) have been employed in controllers [3, 4] to reduce the complexity of infinite-dimensional PDE models. However, since ODEs can only approximate the original system dynamics, closed-loop systems based on ODE models may not necessarily ensure the stability of the original system's response. Consequently, the development of more rigorous designs for control applications, such as endpoint control of flexible manipulators, has garnered research interest [5, 6]. Designing control systems based on precise PDE models allows for higher precision, efficiency, and rigorous stability criteria. Hence, the development of PDE controllers has attracted significant attention. Besides applications in flexible robotics, PDE models are used for modeling and control purposes in fluid dynamics [7], electromagnetics [8], aerospace [9], economics [10], and biology [11]. Therefore, the development of sophisticated PDE control frameworks is beneficial across various fields.

The lack of information on distributed states describing the configuration of a flexible link—such as the displacement of link elements and their higher-order derivatives—poses a significant challenge. Studies focused solely on the control of flexible manipulators often overlook this aspect, assuming that such information is readily measurable [12]. However, this is rarely the case. In practice, only a limited number of measurement samples are incorporated, despite the continuous and infinite-dimensional nature of flexible link dynamics. As a result, the generated mapping for the displacement of the flexible link may be inaccurate in areas not directly covered by measurement points. This limitation prevents the effective implementation of information describing the dynamics of flexible links throughout their length, leading to the in calculability of dynamic terms involving distributed states across the link [13]. In such scenarios, a feasible control input may rely solely on boundary information, which limits control over the distributed states themselves. A potential solution to this problem is the use of state observers [14–17]. However, even studies that incorporate PDE-based estimation strategies often include various simplifications in the dynamic model, as the design of a PDE-based state observer is complex and intensive to implement. Hence, further development of efficient estimation schemes using fewer measurement samples and correspondingly fewer differential equations would significantly enhance control precision and effectiveness.

While the modeling procedure for various classes of infinite-dimensional flexible systems has been extensively documented in the literature [18, 19], incorporating such models into PDE-based controllers remains inherently challenging and cost-intensive. Consequently, approximated ODE models,

such as those based on finite element analysis [20, 21], kernels [22], or assumed-mode methods [23], are often used. To attain more sophisticated design schemes, recent research has adapted alternative strategies where distributed-state estimation is directly incorporated into control calculations. Control and estimation solutions for lower-order PDEs, such as string PDEs [24] and wave PDEs [25], are well-documented in the literature. For instance, Krstic et al. [26] investigated the stabilization of beam equations using a backstepping controller for fourth-order PDEs applicable to beam equations. For systems solely featuring distributed states throughout the length of a flexible beam, Han et al. [27] proposed a boundary controller utilizing distributed states to ensure controller feasibility. In robotic systems featuring additional states beyond those corresponding to beam element deflection, Zhang et al. [28] pioneered a PID-based PDE control design. Subsequent modifications, such as boundary control schemes, have allowed the consideration of additional effects, such as the mitigation of endpoint deflection through exertion of control actions on boundary conditions [29, 30], the consideration of input nonlinearity and backlash effects [31], the investigation of shear deformation effects in Timoshenko beams [32], the control of flexible manipulators in three-dimensional space [33], and the adaptive control of manipulators with unknown control direction [34]. In recent years, neural network-based controllers have been developed for flexible manipulators to conveniently address structured and unstructured uncertainties [1, 35].

Current state-of-the-art model-based control of flexible systems often involves deriving PDE models by assuming the deflections of flexible elements as perfect arcs [31, 36, 37]. This approach results in a set of linear PDEs and boundary conditions that are readily implementable, albeit at the cost of reduced modeling or control precision. Implementing stable and technically sound control schemes using fully nonlinear sets of equations would require significant additional analysis, as conventional numerical techniques based on the separation of variables would not be applicable. Such cases necessitate the direct incorporation of nonlinear PDEs in all design stages. Moreover, the need to recover missing information on distributed states—such as displacement, velocity, and acceleration values for elements of a flexible link—renders the control of systems based on nonlinear PDEs significantly more challenging in flexible robotics. This issue has recently attracted significant attention. Notable examples include an observer design for a flexible manipulator [15], perturbation-based control of flexible two-link systems using state observers [37], and distributed disturbance observers for flexible links [38]. However, the existing literature does not fully incorporate nonlinear PDE-based dynamical models at all design stages of the closed-loop controller-observer system, indicating a need for further development.

## 1.2 | Motivations

The challenge of controlling flexible manipulators, given the limited availability of information, remains a key issue in this field and is still open to study. As flexible mechanisms are inherently distributed systems, their dynamics can only be described using PDE models. In many applications, these models exhibit highly nonlinear and non-homogeneous characteristics

[5]. Nonhomogenous dynamic terms are not strictly functions of distributed states and their higher-order derivatives [6]. Such effects potentially include gravity and control input-based terms acting on boundary conditions of the system. Assigning stable and feasible estimation schemes to such systems requires significant mathematical manipulation. Consequently, relatively simpler formulations with homogeneous boundary conditions and linear deflection models [15, 37, 39] or assumed mode-based estimations of deflections [40, 41] have been used instead. One of the motivations of this study is to develop an appropriate estimation scheme capable of using nonlinear PDE models in a cost-effective manner without introducing superfluous differential equations into the closed-loop system. If distributed states describing the flexible system are available, the real-world problem of precise endpoint control of a flexible manipulator becomes addressable. Current state-of-the-art PDE-based control of flexible systems involves designing control laws to ensure the decay of a corresponding Lyapunov function that includes state-tracking and displacement effects [5, 28, 29]. However, obtaining such control laws can be challenging when using more complex mathematical models or may require reductive strategies, such as the separation of variables, to be incorporated into the controller design [2]. An alternative strategy involves dividing the overall system into “slow” (planar motion of the manipulator) and “fast” (deflection of flexible link elements) counterparts using perturbation methods [37]. However, this method conventionally does not account for the interactions between the two subsystems. Therefore, proposing a nonlinear PDE control scheme that features precise dynamical models and considers interactions between various distributed states and planar motion is the second motivation of this work. In addition, a rigorous stability analysis of the PDE system described by a system of nonlinear PDEs requires in-depth investigation based on Lyapunov stability theory and the extended LaSalle’s invariance principle for infinite-dimensional systems [5, 42], which must be adapted to the corresponding nonlinear mapping.

### 1.3 | Novelties

Based on the shortcomings in the current state-of-the-art, this article investigates the problem of endpoint control and distributed-state estimation of nonlinear flexible systems. The major contributions of this work are summarized as follows: (i) A novel partial state observer is proposed, which enables estimating link deflections using a nonlinear PDE model without significantly increasing design and implementation complexity. (ii) The feasibility of the observer is ensured based on a novel Lyapunov function using appropriate control parameters and the calculation of observer input to ensure asymptotic stability and convergence to the original states. (iii) A new nonlinear PDE-based boundary control scheme is presented for endpoint and state tracking and the elimination of endpoint deflection based on distributed estimations. (iv) A framework for stability analysis of the closed-loop system is presented based on the extended LaSalle’s invariance principle for infinite-dimensional system, which incorporates a new semi-linear mapping. (v) Control structure enables straightforward implementation of multi-input-multi-output (MIMO) design, as well as implementation for parametrically uncertain systems based on its adaptive

design. (vi) The nonlinear PDE model of the flexible system is considered at all stages of constructing the feedback loop, with no simplification in manipulations corresponding to the PDE model.

The rest of this paper is organized as follows. Section 2 discusses problem preliminaries and presents the mathematical model of the flexible system. Section 3 details the construction of a distributed-state observer for the recovery of missing states. The design and analysis of the nonlinear PDE controller are featured in Section 4. Finally, Section 5 demonstrates the efficiency and precision of the proposed schemes based on numerical simulations.

## 2 | Problem Statement and Preliminaries

To investigate the control of flexible robotic manipulators, a standard system of a one-link robotic arm [43] is considered. The mechanism consists of a flexible link in the vertical plane, as depicted in Figure 1. In this paper, the flexible arm is modeled as an infinite-dimensional beam with distributed displacement states  $\omega(\xi)$ , where  $\xi$  indicates the position of an element of the flexible beam alongside its longitudinal axis. The variable  $t$  represents the system time. The parameters  $l$ ,  $A$ ,  $\rho$ ,  $E$ , and  $I$ , respectively, denote the length, cross-sectional area, mass density, elastic modulus, and second moment of area of the beam. The angle  $\theta$  expresses the angle of the beam with respect to the designated  $\langle x, y \rangle$  coordinate system. A lumped mass  $M$  is installed at the end of the flexible beam and acts as the payload of the mechanism. An input torque  $\tau$  is exerted at joint  $O$ , and a boundary input force  $F_b$  is applied to the endpoint of the beam located at  $\xi = l$ .

**Assumption 1.** It is assumed that the effects of longitudinal displacement of the beam are negligible, as no distributed axial force is exerted on the system. On this basis,  $F_b$  is considered perpendicular to  $r_l$ , which represents  $r_\xi$  for  $\xi = l$ . The perpendicular component of the input acts as a shear force on boundary condition. For general applications, if the input force is exerted in another direction, only the component of the force perpendicular to  $r_l$  is incorporated into the design.

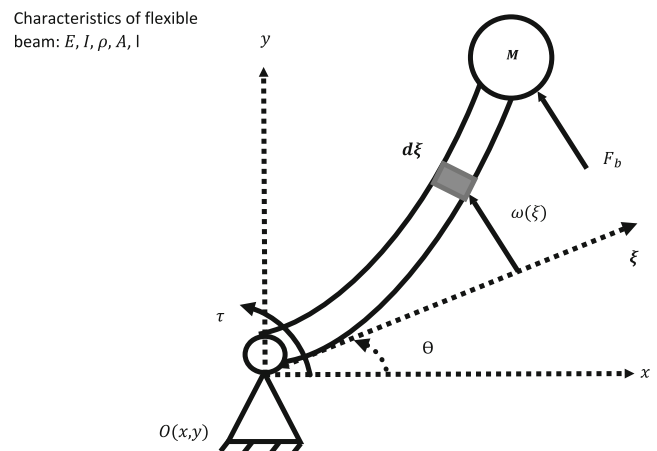


FIGURE 1 | Schematic of a flexible arm with payload.

The extended Hamilton principle [18] is used in this study to obtain the mathematical model for the described dynamical system. To this end, the position vector  $\mathbf{r}_\xi$  for an infinitesimal element of the flexible beam located at coordinate  $\xi$  with respect to the connecting joint and the position vector  $\mathbf{r}_M$  for the payload are expressed in (1–4). The volumetric density of the beam is expressed as  $\rho$ . The cross-sectional area of the beam is indicated by  $A$ . The mass of flexible beam is expressed as  $m \triangleq \rho A l$ . The moment of inertia of the joint is expressed by  $I_h$ .

$$\mathbf{r}_\xi = \begin{bmatrix} r_{x,\xi} \\ r_{y,\xi} \end{bmatrix} \quad (1)$$

$$r_{x,\xi} = \xi \cos \theta - \omega(\xi) \sin \theta \quad (2)$$

$$r_{y,\xi} = \xi \sin \theta + \omega(\xi) \cos \theta \quad (3)$$

$$\mathbf{r}_M = \mathbf{r}_l \quad (4)$$

According to the Euler–Bernoulli beam theory, the kinetic energy  $T$ , potential energy  $V$ , and generalized force corresponding to the entire mechanism are described as follows:

$$\begin{aligned} T = & \frac{1}{2} I_h \dot{\theta}^2 + \frac{1}{2} \rho A \int_0^l \dot{\mathbf{r}}_\xi^T \dot{\mathbf{r}}_\xi d\xi + \frac{1}{2} M \dot{\mathbf{r}}_l^T \dot{\mathbf{r}}_l = \frac{1}{2} I_m \dot{\theta}^2 \\ & + \frac{1}{2} \rho A \int_0^l \left[ \dot{\omega}^2(\xi) + \omega^2(\xi) \dot{\theta}^2 + 2\xi \dot{\theta} \dot{\omega}(\xi) \right] d\xi \\ & + \frac{1}{2} M \left[ l^2 \dot{\theta}^2 + \dot{\omega}^2(l) + \omega^2(l) \dot{\theta}^2 + 2l \dot{\theta} \dot{\omega}(l) \right] \end{aligned} \quad (5)$$

$$V = \frac{1}{2} m g l \sin \theta + M g l \sin \theta + M g \omega(l) \cos \theta + \frac{1}{2} E I \left[ \frac{\partial^2 \omega(\xi)}{\partial \xi^2} \right]^2 d\xi \quad (6)$$

$$Q_\theta = \tau \frac{\partial \mathbf{r}_O}{\partial \theta} + F_b \frac{\partial \mathbf{r}_l}{\partial \theta} \quad (7)$$

The mass moment of inertia of the system constituted of joint and beam rigid beam with identical density and geometric properties are expressed as  $I_m = I_h + \frac{1}{3} \rho A l^3$ . For brevity, expressions  $\omega_\xi = \frac{\partial \omega}{\partial \xi}$  and  $\omega_l = \frac{\partial \omega}{\partial l}$  are used to express partial derivatives of distributed states. Notation  $[\dot{\cdot}]$  represents the derivative of the bracketed term with respect to time, while  $[-']$  denotes the derivative of the bracketed term with respect to position.

Next, the variation terms for (5–7) are calculated for substitution in the extended Hamilton principle  $\delta(T - V + Q) = 0$  as follows:

$$\begin{aligned} \delta \int_{t_1}^{t_2} T dt = & \int_{t_1}^{t_2} \left\{ \left\{ -I_m \ddot{\theta} - M l^2 \ddot{\theta} - M \omega^2(l) \ddot{\theta} - 2M \omega(l) \omega_l(l) \dot{\theta} \right. \right. \\ & - M \omega_{ll}(l) + \rho A \int_0^l \left[ -2\omega(\xi) \omega_l(\xi) \dot{\theta} - \omega^2(\xi) \ddot{\theta} - \xi \omega_{ll}(\xi) \right] d\xi \left. \right\} \delta \theta \\ & + \left\{ \rho A \int_0^l \left[ -\omega_{ll}(\xi) + \omega(\xi) \dot{\theta}^2 - \xi \ddot{\theta} \right] d\xi \right\} \delta \omega(\xi) \\ & + \left[ -M \omega_{ll}(l) + M \omega(l) \dot{\theta}^2 - M l \ddot{\theta} \right] \delta \omega(l) \left. \right\} dt \end{aligned} \quad (8)$$

$$\begin{aligned} \delta \int_{t_1}^{t_2} V dt = & \int_{t_1}^{t_2} \left\{ \left[ \frac{1}{2} m g l \cos \theta + M g l \cos \theta - M g \sin \theta \omega(l) \right] \delta \theta \right. \\ & + \left[ -E I \omega_{\xi\xi\xi\xi} + M g \cos \theta \right] \delta \omega(l) + E I \omega_{\xi\xi} \delta \omega'(l) \\ & \left. - E I \omega_{\xi\xi} \delta \omega'(0) + E I \omega_{\xi\xi\xi} \delta \omega(0) + E I \int_0^l \omega_{\xi\xi\xi\xi} d\xi \delta \omega(\xi) \right\} dt \end{aligned} \quad (9)$$

$$\delta W = (\tau + F_b l) \delta \theta + u \delta \omega(l) \quad (10)$$

Then, the mathematical model for the system dynamics, including the governing equations and boundary conditions, is obtained as (11–15).  $d_1$  and  $d_2$  indicate input disturbance and unmodeled dynamic terms.

$$\begin{aligned} & [I_m + M l^2 + M \omega^2(l)] \ddot{\theta} + M l \omega_{ll}(l) + 2M \omega(l) \omega_l(l) \dot{\theta} \\ & + \rho A \int_0^l \left[ 2\omega(\xi) \omega_l(\xi) \dot{\theta} + \omega^2(\xi) \ddot{\theta} + \xi \omega_{ll}(\xi) \right] d\xi \\ & + \frac{1}{2} m g l \cos \theta + M g l \cos \theta - M g \omega(l) \sin \theta = \tau + F_b l + d_1 \end{aligned} \quad (11)$$

$$\omega_{ll}(\xi) - \omega(\xi) \dot{\theta}^2 + \xi \ddot{\theta} + \frac{E I}{\rho A} \omega_{\xi\xi\xi\xi}(\xi) = 0 \quad (12)$$

$$\omega_{ll}(l) - \omega(l) \dot{\theta}^2 + l \ddot{\theta} + g \cos \theta - \frac{E I}{M} \omega_{\xi\xi\xi}(l) = \frac{1}{M} F_b + d_2 \quad (13)$$

$$\omega(0) = \omega_\xi(0) = 0 \quad (14)$$

$$\omega_{\xi\xi}(l) = 0 \quad (15)$$

**Remark 1. (control objectives).** The following control objectives are considered:

- i. tracking of the position reference signal  $\theta_r$  with respect to system state  $\theta$ ;
- ii. elimination of endpoint deflection, resulting in the tracking of desired endpoint trajectory  $(x_{l,r}, y_{l,r})$ ;
- iii. mitigating link deflection  $\omega(\xi)$ ,  $\xi \in [0, l]$  and ensuring its boundedness.

As such, a closed-loop system would feature two input signals—i.e., joint torque  $\tau$  and boundary input  $F_b$  as well as outputs  $\theta$  and  $\omega(\xi)$ ,  $\xi \in [0, l]$ . It is desired that the controller is assigned such that it enables convenient investigation of interactions between multiple inputs and outputs in a MIMO framework.

**Remark 2. (significance of boundary control strategy).**

The control system is heavily underactuated. In other words, a limited number of inputs are used to attain infinite objectives due to the existence of distribution states. Hence, to attain all control objectives, an input force is extended to the endpoint in addition to input torque at the joint. This approach enables the elimination of endpoint deflection and tracking joint reference, modeled as a fully actuated subsystem in Section 4. Then, based on the analysis of closed-loop system response and assigned Lyapunov function, it will be demonstrated that this

structure results in the elimination of link deflection, which satisfies the objective of distributed state control. In other words, exertion of the boundary input force allows for a rigorous—and not heuristic—design procedure. This strategy has been adapted in the latest developments in the field of PDE control of flexible systems [29] where control action is exerted unto boundary conditions. To implement boundary inputs in practical applications and experiments, hydraulic or pneumatic actuators connected to the endpoint of the manipulator using nozzles may be employed [44].

**Assumption 2.** It is considered that information on distributed states is not available. In other words, deflections and their temporal and spatial derivatives are not known. This assumption is valid as measuring continuous displacement through the length of a flexible beam is not practical in many applications due to the need for the application of a large number of sensors and advanced measurement technology. Furthermore, calculating higher-order time derivatives of displacement states is cost-intensive and potentially inaccurate. Hence, the estimation of the mentioned states is required for precise control of the flexible system.

**Assumption 3.** State  $\theta$  is considered as measurable. Joint angle is easily measurable using conventional measurement devices such as encoders. This assumption is significant in improving the feasibility of the estimation scheme as it allows forgoing corresponding error dynamics in observer design.

**Assumption 4.** As longitudinal deflection of the beam is considered negligible in this study according to Assumption 1, the uncertainty of the length of the manipulator  $l$  is assumed to be negligible. Uncertainty in input term  $\frac{1}{M}F_b$  is incorporated in  $d_2$ . However, results obtained in this paper will be also applicable to manipulators with varying lengths in case appropriate modifications in the original model are conducted [45, 46].

**Assumption 5.** To compensate for the effects of potential parametric uncertainty, control action is designed such that it features parametric adaptation. To this end, the system parameter vector is defined as follows:

$$s = [M, s_1, s_2, m]^T \quad (16)$$

where  $s_1 = \frac{EI}{\rho A}$  and  $s_2 = \frac{EI}{M}$ . The estimated parameter vector  $\hat{s}$  is used in the construction of the control scheme. Additionally, it is assumed that  $s$  is bounded according to Assumption 6.

**Assumption 6.** The assigned uncertainty space is defined as  $\mathcal{Q} = \{s \in \mathbb{R}^4 : s_l < s < s_h\}$ .  $s_l$  and  $s_h$  are respectively lower and upper bounds for  $s$ , which are assumed to be known.

Based on the definition of  $\bar{s}$ , all elements of  $\bar{s}_l$  and  $\bar{s}_h$  attain strictly positive values. The parametric estimation error is defined as follows:

$$\tilde{s} = s - \hat{s} \quad (17)$$

On this basis, a projection function with respect to uncertainty space  $\mathcal{Q}$  is assignable for given values  $s$ ,  $s_l$ ,  $s_h$ , and  $e$ , where  $s_l$

and  $s_h$  indicate lower and upper uncertainty bounds for  $s$ .

$$\mathcal{P}(s, s_l, s_h, e) = \begin{cases} 0, & \text{if } \mathcal{P} \geq s_h \text{ and } e > 0 \\ 0, & \text{if } \mathcal{P} \leq s_l \text{ and } e < 0 \\ e, & \text{otherwise} \end{cases} \quad (18)$$

**Lemma 1.** If  $\hat{s} = \mathcal{P}(\hat{s}, s_l, s_h, e)$  is assigned, the following holds:

$$s_l < \hat{s} < s_h \quad (19)$$

$$(s - \hat{s})[e - \mathcal{P}(\hat{s}, s_l, s_h, e)] \leq 0 \quad (20)$$

*Proof.* The proof is a standard property of projection functions [13] and is omitted.

### 3 | PDE-Based Distributed State Observer

This section details the construction of a novel distributed state observer using limited boundary measurements based on the nonlinear PDE-based mathematical model described in (8–12). The estimate of  $\omega(\xi)$  is denoted as  $\hat{\omega}(\xi)$ .

A partial state observer (21–26) is proposed in this work.

$$\begin{aligned} & [\hat{I}_m + \hat{M}l^2 + \hat{M}\hat{\omega}^2(l)]\ddot{\theta} + \hat{M}l\hat{\omega}_{tt}(l) + 2\hat{M}\hat{\omega}(l)\hat{\omega}_t(l)\dot{\theta} \\ & + \hat{\rho}\hat{A}\int_0^l [2\hat{\omega}(\xi)\hat{\omega}_t(\xi)\dot{\theta} + \hat{\omega}^2(\xi)\ddot{\theta} + \xi\hat{\omega}_{tt}(\xi)]d\xi \\ & + \frac{1}{2}\hat{m}g\hat{l}\cos\theta + \hat{M}gl\cos\theta - \hat{M}g\hat{\omega}(l)\sin\theta = \tau + F_b l + d_1 \end{aligned} \quad (21)$$

$$\hat{\omega}_{tt}(\xi) - \hat{\omega}(\xi)\dot{\theta}^2 + \xi\ddot{\theta} + s_1\hat{\omega}_{\xi\xi\xi\xi}(\xi) = 0 \quad (22)$$

$$\hat{\omega}_{tt}(l) - \hat{\omega}(l)\dot{\theta}^2 + l\ddot{\theta} + g\cos\theta - s_2\hat{\omega}_{\xi\xi\xi}(l) + u_{ob} = \frac{1}{M}F_b + d_2 \quad (23)$$

$$\hat{\omega}(0) = \hat{\omega}_{\xi}(0) = 0 \quad (24)$$

$$\hat{\omega}_{\xi\xi}(l) = 0 \quad (25)$$

$$z(\xi) = \omega(\xi) - \hat{\omega}(\xi) \quad (26)$$

$u_{ob}$  is the observer input and  $z(\xi)$  is the estimation error. To investigate the error dynamics of the observer, (12–15) and (22–25) will be analyzed as  $\theta$  is assumed to be measurable.

Assigning  $\omega(\xi) = \hat{\omega}(\xi) + z(\xi)$ , error dynamics of the observer is expressed as follows:

$$z_{tt}(\xi) - \dot{\theta}^2 z(\xi) + s_1 z_{\xi\xi\xi\xi}(\xi) = 0 \quad (27)$$

$$z_{tt}(l) - \dot{\theta}^2 z(l) - s_2 z_{\xi\xi\xi}(l) + d_o = u_{ob} \quad (28)$$

$$z(0) = z_{\xi}(0) = 0 \quad (29)$$

$$z_{\xi\xi}(l) = 0 \quad (30)$$

The term  $d_o$  describes compound disturbance effects acting on (28) and is expressible as  $d_o \in \mathcal{D}_o \triangleq \{d_o \in \mathbb{R} : d_{ol} < d_o < d_{oh}\}$ .  $\mathcal{D}_o$  is the corresponding uncertainty space.

**Theorem 1.** PDE observer (21–26) is asymptotically stable—that is,  $\hat{\omega}(\xi) \rightarrow \omega(\xi)$  and  $\hat{\omega}_i(\xi) \rightarrow \omega_i(\xi)$  for  $\xi \in [0, l]$ —in case decision variables  $p$ ,  $\alpha$ , and  $\beta$  and observer input signal  $u_{ob}$  satisfy the following conditions.

$$\max(\beta^2 + \alpha^2 \theta^2 - p\alpha\beta, \beta^2 + \alpha^2 \theta^2 - p\alpha\beta \theta^2) \leq 0 \quad (31)$$

$$\begin{aligned} & -\delta\alpha\beta\hat{s}_1 \left[ -z_{\xi\xi\xi}(l) - 2z_{\xi\xi\xi}(0) + \frac{2}{l}z_\xi^2(l) \right] - \alpha^2\hat{s}_1 z_t(l)z_{\xi\xi\xi}(l) \\ & - \theta^2 z_t(l)z(l) + \hat{s}_2 z_t(l)z_{\xi\xi\xi}(l) + z(l)z_t(l) + \xi_{ob} - u_{ob}z_t(l) < 0 \end{aligned} \quad (32)$$

$$0 < \delta < p \quad (33)$$

$$\hat{s} = \mathcal{P}(s, s_l, s_h, \lambda_Q) \quad (34)$$

$\lambda_Q$  and  $\xi_{ob}$  are assigned with respect to uncertainty space  $\mathcal{Q}$ .

*Proof.* The following candidate Lyapunov function (CLF) is considered for the distributed-state observer.

$$V_{ob} = V_n + V_s \quad (35)$$

$$V_n = \int_0^l \frac{1}{2} \alpha^2 s_1 z_{\xi\xi}^2 d\xi + \mathcal{K}_n + V_s + \frac{1}{2} z^2(l) + \frac{1}{2} z_t^2(l), \text{ for } i = 1, 2 \quad (36)$$

$$\mathcal{K}_n = \int_0^l \left\{ \frac{1}{2} \alpha^2 z_t^2 + \frac{1}{2} \beta^2 z^2 + \alpha\beta\delta \left( -2 + \frac{\xi}{l} \right) z z_t \right\} d\xi \quad (37)$$

$$V_s = \frac{1}{2} \gamma \bar{s}^T \bar{s} \quad (38)$$

To demonstrate  $V_{ob} \geq 0$ , it is noted that  $\int_0^l \left\{ \frac{1}{2} \alpha^2 z_t^2 + \frac{1}{2} \beta^2 z^2 + \alpha\beta \left( -2 + \frac{\xi}{l} \right) z z_t \right\} d\xi \geq \int_0^l \left\{ \frac{1}{2} \alpha^2 z_t^2 + \frac{1}{2} \beta^2 z^2 - 2\alpha\beta |z| |z_t| \right\} d\xi \geq \frac{1}{2} \int_0^l (|\alpha z_t| - |\beta z|)^2 d\xi \geq 0$ . Hence,  $\int_0^l \delta\alpha\beta \left( -2 + \frac{\xi}{l} \right) z z_t d\xi \geq \int_0^l \left\{ -\frac{1}{2} \delta\alpha^2 z_t^2 - \frac{1}{2} \delta\beta^2 z^2 \right\} d\xi$ . Adding  $\frac{1}{2} \int_0^l \left\{ \alpha^2 z_t^2 + \beta^2 z^2 \right\} d\xi$  to both sides, it is obtained that  $\mathcal{K}_n = \int_0^l \left\{ \frac{1}{2} \alpha^2 z_t^2 + \frac{1}{2} \beta^2 z^2 + \alpha\beta\delta \left( -2 + \frac{\xi}{l} \right) z z_t \right\} d\xi \geq \left( \frac{1}{2} - \delta \right) \int_0^l \left\{ \alpha^2 z_t^2 + \beta^2 z^2 \right\} d\xi \geq 0$ . Following the same procedure, an upper bound for  $\mathcal{K}_n$  is demonstrated as  $\mathcal{K}_n \leq \left( \frac{1}{2} + \delta \right) \int_0^l \left\{ \alpha^2 z_t^2 + \beta^2 z^2 \right\} d\xi$ . Hence, it is written that

$$0 \leq \left( \frac{1}{2} - \delta \right) \int_0^l \left\{ \alpha^2 z_t^2 + \beta^2 z^2 \right\} d\xi \leq \mathcal{K}_n \leq \left( \frac{1}{2} + \delta \right) \int_0^l \left\{ \alpha^2 z_t^2 + \beta^2 z^2 \right\} d\xi \quad (39)$$

Therefore,  $V_{ob} > 0$ .

To prove the robustness of the system in the presence of parametric uncertainty, we begin by analyzing the case where the perturbation term  $\bar{s} = \mathbf{0}$ . Subsequently, we demonstrate the boundedness of the system response when modeling uncertainty is present.

Time derivative of  $V_n$  will be investigated in the rest of the proof.

$$\begin{aligned} \dot{V}_n = & \int_0^l \left\{ \alpha^2 z_t z_{tt} + \alpha^2 s_1 z_{\xi\xi} z_{\xi\xi t} + \beta^2 z z_t + \delta\alpha\beta \left( -2 + \frac{\xi}{l} \right) z_t^2 \right. \\ & \left. + \delta\alpha\beta \left( -2 + \frac{\xi}{l} \right) z z_{tt} \right\} d\xi + \frac{1}{2} z(l)z_t(l) + \frac{1}{2} z_t(l)z_{tt}(l) \end{aligned} \quad (40)$$

Substituting (27–30) in (40), it follows that

$$\begin{aligned} \dot{V}_n = & \left( \beta^2 + \alpha^2 \theta^2 \right) \int_0^l z_t z d\xi - \alpha^2 s_1 \int_0^l z_t z_{\xi\xi\xi\xi} d\xi \\ & - \alpha^2 \bar{s}_1 \int_0^l z_t \hat{\omega}_{\xi\xi\xi\xi} d\xi - \alpha^2 s_1 z_t z_{\xi\xi\xi}(l) - \alpha^2 s_1 z_{\xi\xi\xi} z_{t\xi}(0) \\ & + \alpha^2 s_1 \int_0^l z_t z_{\xi\xi\xi\xi} d\xi + \delta\alpha\beta \int_0^l \left( -2 + \frac{\xi}{l} \right) z_t^2 d\xi \\ & + \delta\alpha\beta \theta^2 \int_0^l \left( -2 + \frac{\xi}{l} \right) z^2 d\xi - \delta\alpha\beta s_1 \int_0^l \left( -2 + \frac{\xi}{l} \right) z z_{\xi\xi\xi\xi} d\xi \\ & - \delta\alpha\beta \bar{s}_1 \int_0^l \left( -2 + \frac{\xi}{l} \right) z \hat{\omega}_{\xi\xi\xi\xi} d\xi + z(l)z_t(l) - \theta^2 z(l)z_t(l) \\ & + s_2 z_{\xi\xi\xi}(l)z_t(l) + \bar{s}_2 \hat{\omega}_{\xi\xi\xi}(l)z_t(l) + z(l)z_t(l) - u_{ob}z_t(l) \\ & + d_o z_t(l) + \gamma \bar{s}^T \bar{s} \end{aligned} \quad (41)$$

Next, higher-order terms will be integrated into parts.

$$\begin{aligned} \dot{V}_n = & \left( \beta^2 + \alpha^2 \theta^2 \right) \int_0^l z_t z d\xi + \delta\alpha\beta \int_0^l \left( -2 + \frac{\xi}{l} \right) z_t^2 d\xi \\ & + \delta\alpha\beta \theta^2 \int_0^l \left( -2 + \frac{\xi}{l} \right) z^2 d\xi - \delta\alpha\beta s_1 \int_0^l \left( -2 + \frac{\xi}{l} \right) z_{\xi\xi}^2 d\xi \\ & - \delta\alpha\beta s_1 \left[ -z_{\xi\xi\xi}(l) - 2z_{\xi\xi\xi}(0) + \frac{2}{l}z_\xi^2(l) \right] - \alpha^2 s_1 z_t z_{\xi\xi\xi}(l) \\ & - \theta^2 z(l)z_t(l) + s_2 z_{\xi\xi\xi}(l)z_t(l) + z(l)z_t(l) + \bar{s}_2 \hat{\omega}_{\xi\xi\xi}(l)z_t(l) \\ & - u_{ob}z_t(l) + d_o z_t(l) + \xi_{ob} - \alpha^2 \bar{s}_1 \int_0^l z_t \hat{\omega}_{\xi\xi\xi\xi} d\xi \\ & - \delta\alpha\beta \bar{s}_1 \int_0^l \left( -2 + \frac{\xi}{l} \right) z \hat{\omega}_{\xi\xi\xi\xi} d\xi \end{aligned} \quad (42)$$

The unmodeled disturbance term  $\xi_{ob}$  is assigned as  $\xi_{ob} = \text{Sup}_{\mathcal{D}_o} \{d_o z_t(l)\}$  in order to express (42) in robust form. The term  $\text{Sup}_{\mathcal{D}_o}[-]$  indicates supremum of bracketed term over  $\mathcal{D}_o$ .

Using Cauchy–Schwarz inequality, it follows that

$$\begin{aligned} \dot{V}_n \leq & \left( \beta^2 + \alpha^2 \theta^2 \right) \int_0^l z^2 d\xi + \left( \beta^2 + \alpha^2 \theta^2 \right) \int_0^l z_t^2 d\xi \\ & + \delta\alpha\beta \int_0^l \left( -2 + \frac{\xi}{l} \right) z_t^2 d\xi + \delta\alpha\beta \theta^2 \int_0^l \left( -2 + \frac{\xi}{l} \right) z^2 d\xi \\ & - \delta\alpha\beta \frac{EI}{\rho A} \int_0^l \left( -2 + \frac{\xi}{l} \right) z_{\xi\xi}^2 d\xi \\ & - \delta\alpha\beta \frac{EI}{\rho A} \left[ -z_{\xi\xi\xi}(l) - 2z_{\xi\xi\xi}(0) + \frac{2}{l}z_\xi^2(l) \right] + \xi_{ob} \\ & - \alpha^2 \frac{EI}{\rho A} z_t z_{\xi\xi\xi}(l) - \theta^2 z_t(l)z(l) + \frac{EI}{M} z_t(l)z_{\xi\xi\xi}(l) \\ & + z(l)z_t(l) - u_{ob}z_t(l) \end{aligned} \quad (43)$$

As  $\delta\left(-2 + \frac{\xi}{l}\right)z^2 \leq -pz^2$  and  $\delta\left(-2 + \frac{\xi}{l}\right)z_l^2 \leq -pz_l^2$ , (A.7) will be further simplified as (44).

$$\dot{V}_n \leq \gamma_n \quad (44)$$

$$\begin{aligned} \gamma_n = & \left(\beta^2 + \alpha^2\dot{\theta}^2 - p\alpha\beta\dot{\theta}^2\right) \int_0^l z^2 d\xi \\ & + \left(\beta^2 + \alpha^2\dot{\theta}^2 - p\alpha\beta\right) \int_0^l z_l^2 d\xi - \delta\alpha\beta s_1 \int_0^l \left(-2 + \frac{\xi}{l}\right) z_{\xi\xi}^2 d\xi \\ & - \delta\alpha\beta s_1 \left[-z_{\xi\xi\xi}(l) - 2z_{\xi\xi\xi}(0) + \frac{2}{l}z_{\xi\xi}^2(l)\right] - \alpha^2 s_1 z_l z_{\xi\xi\xi}(l) \\ & - \dot{\theta}^2 z_l(l)z(l) + s_2 z_l(l)z_{\xi\xi\xi}(l) + z(l)z_l(l) + \xi_{ob} - u_{ob}z_l(l) \end{aligned} \quad (45)$$

To demonstrate conditions for the decay of the Lyapunov function, it is noted that.

$$\beta^2 + \alpha^2\dot{\theta}^2 - p\alpha\beta\dot{\theta}^2 \leq \beta^2 + \alpha^2\dot{\theta}^2 - p\alpha\beta, \quad \text{if } |\dot{\theta}| \geq 1 \quad (46)$$

$$\beta^2 + \alpha^2\dot{\theta}^2 - p\alpha\beta\dot{\theta}^2 > \beta^2 + \alpha^2\dot{\theta}^2 - p\alpha\beta, \quad \text{if } |\dot{\theta}| < 1 \quad (47)$$

Finally, it is shown that (46) and (47) are solvable for the corresponding condition. To do this, the parameter transformation  $\beta = \alpha$  is assigned. Substituting this expression, the stability conditions for the observer are re-expressed as

$$c^2 - pc + \dot{\theta}^2 < 0, \quad \text{if } |\dot{\theta}| \geq 1 \quad (48)$$

$$c^2 - p\dot{\theta}^2 c + \dot{\theta}^2 > 0, \quad \text{if } |\dot{\theta}| < 1 \quad (49)$$

As (49)  $c^2 - p\dot{\theta}^2 c + \dot{\theta}^2 > c^2 - pc + \dot{\theta}^2$  for  $|\dot{\theta}| < 1$ , (49) is relaxed as follows:

$$c^2 - pc + \dot{\theta}^2 > 0, \quad \text{if } |\dot{\theta}| < 1 \quad (50)$$

Considering (48) and (50) as second-order inequality for  $c$ , a feasible solution exists if discriminant  $q$  of the left-hand side is positive. This condition is expressed as follows:

$$q = p^2 - 4\dot{\theta}^2 > 0 \quad (51)$$

Hence, feasible values for  $p$  are expressible as in (52).

$$p > 2\dot{\theta} \quad (52)$$

Then, based on (42–47), the stability conditions (31–33) are obtained with feasible solutions for (52).

In order to demonstrate the boundedness of estimation error, on the one hand, it is noted from (44) that

$$\dot{V}_n \leq -\epsilon_1 \int_0^l z^2 d\xi - \epsilon_2 \int_0^l z_l^2 d\xi - \epsilon_3 \int_0^l z_{\xi\xi}^2 d\xi \quad (53)$$

$$\epsilon_1 = \beta^2 + \alpha^2\dot{\theta}^2 - p\alpha\beta\dot{\theta}^2 \quad (54)$$

$$\epsilon_2 = \beta^2 + \alpha^2\dot{\theta}^2 - p\alpha\beta \quad (55)$$

$$\epsilon_3 = \delta\alpha\beta s_1 \quad (56)$$

On the other hand, the following holds true based on (36):

$$V_n > \epsilon_1 \int_0^l z^2 d\xi + \epsilon_2 \int_0^l z_l^2 d\xi + \epsilon_3 \int_0^l z_{\xi\xi}^2 d\xi \quad (57)$$

$$\epsilon_1 = \frac{1}{2p}(p - \delta)\beta^2 \quad (58)$$

$$\epsilon_2 = \frac{1}{2p}(p - \delta)\alpha^2 \quad (59)$$

$$\epsilon_3 = \frac{1}{2}\alpha^2 s_1 \quad (60)$$

Hence, from (53) and (57), it follows that Lyapunov function  $V_n$  is decaying as in (61).

$$\dot{V}_n < -\sigma_n V_n \quad (61)$$

where  $\sigma_n = \min(\epsilon_1, \epsilon_2, \epsilon_3) / \max(\epsilon_1, \epsilon_2, \epsilon_3)$ .

To address parametric uncertainty, the time derivative of  $V_s$  is investigated as follows:

$$\dot{V}_s = \tilde{s}^T \dot{\tilde{s}} = (s - \hat{s})^T (s - \dot{\hat{s}}) = -\dot{\tilde{s}}^T (s - \hat{s}) \quad (62)$$

Combining (35), (44), and (62) leads to

$$\begin{aligned} \dot{V}_{ob} = & \dot{V}_n + \dot{V}_s \leq \gamma_n + \tilde{s}_2 z_l(l) z_{\xi\xi\xi}(l) \\ & - \delta\alpha\beta \tilde{s}_1 \int_0^l \left(-2 + \frac{\xi}{l}\right) z_{\xi\xi}^2 d\xi - \dot{\tilde{s}}^T \tilde{s} \leq \hat{\gamma}_n + \tilde{\gamma}_n \\ & + \tilde{s}_2 z_l(l) z_{\xi\xi\xi}(l) - \delta\alpha\beta c_f \tilde{s}_1 \int_0^l \left(-2 + \frac{\xi}{l}\right) \hat{\omega}_{\xi\xi}^2 d\xi \\ & - \dot{\tilde{s}}^T \tilde{s} \leq \hat{\gamma}_n + \lambda_{s_1} \tilde{s}_1 + \lambda_{s_2} \tilde{s}_2 - \dot{\tilde{s}}^T \tilde{s} \end{aligned} \quad (63)$$

$$\lambda_{s_1} = 2\delta\alpha\beta c_f \text{Sup} \left[ \int_0^l \hat{\omega}_{\xi\xi}^2 d\xi \right] \quad (64)$$

$$\lambda_{s_2} = z_l(l) z_{\xi\xi\xi}(l) \quad (65)$$

where  $\hat{\gamma}_n$  is the estimation of  $\gamma_n$  using estimated system parameters expressed in Assumption 6 and  $\tilde{\gamma}_n = \gamma_n - \hat{\gamma}_n$  is the estimation error for  $\gamma_n$ . From Assumption 6, it follows that  $\tilde{\gamma}_n$  is expressible as a function of  $\tilde{s}$ , with its upper bound expressible as  $\lambda_{\tilde{Q}}^T \tilde{s}$ , where  $\lambda_{\tilde{Q}} \in \mathbb{R}^4$ . Assigning  $\text{Sup} \left[ \int_0^l z_{\xi\xi}^2 d\xi \right] < c_o \int_0^l \hat{\omega}_{\xi\xi}^2 d\xi$  for a  $c_o > 0$  (which is assignable based on investigation of maximum deflection of the link, or may be assigned an arbitrarily large value), the term  $\lambda_{s_1} \tilde{s}_1 + \lambda_{s_2} \tilde{s}_2 - \dot{\tilde{s}}^T \tilde{s}$  is rewritten in vector form as follows:

$$\lambda_{s_1} \tilde{s}_1 + \lambda_{s_2} \tilde{s}_2 + \lambda_{\tilde{Q}}^T \tilde{s} - \dot{\tilde{s}}^T \tilde{s} = \left( \Lambda_s + \lambda_{\tilde{Q}}^T - \dot{\tilde{s}} \right)^T \tilde{s} \quad (66)$$

$$\Lambda_s = \left[ \lambda_{s_1}, \lambda_{s_2}, 0, 0 \right]^T \quad (67)$$

Substituting (66) and parameter update rule (34) in (63) and then using Lemma 1 leads to

$$\dot{V}_{ob} \leq -\sigma_n V_n + \left[ \Lambda_s - \mathcal{P}(s, s_l, s_h, \lambda_{\tilde{Q}}) \right]^T \tilde{s} \leq -\sigma_n V_n \quad (68)$$

It follows that  $V_{ob}(t) < V_{ob}(0) \exp \int_0^t -\sigma_{ob}(t)dt$ . Additionally, from (35) and (39), it holds that  $\int_0^l z^2 d\xi < \frac{1}{2}(1 + \delta)\beta^2 V_{ob}$ . Hence, the estimation error term is bounded such that  $\int_0^l z^2 d\xi < \frac{1}{2}(1 + \delta)\beta^2 V_{ob}(0) \exp \int_0^t -\sigma_{ob}(t)dt$  and decays to zero with  $t \rightarrow \infty$ . This completes the proof.

**Remark 3. (practicality of observer).** The proposed observer (22–26) is practical as all required feedback is measurable or calculable using standard devices and methods. State  $\theta$  is measurable using standard joint angle sensors.  $\omega(l)$  and  $\omega_t(l)$  are also obtainable from endpoint measurements. Higher-order derivative term  $\omega_{\xi\xi\xi}(l)$  is estimable using strain gauges as  $\omega_{\xi\xi\xi}(l) \approx [\omega_{\xi\xi}(l) - \omega_{\xi\xi}(l - \Delta l)] / l$ —where  $l - \Delta l$  indicates the measurement sample closest to the endpoint of the link [47]—or based on numerical backward derivative using position data obtained using measurement data obtained from sensors such as inertial measurement units or optic ground-truth systems [6] as  $\omega_{\xi\xi\xi}(l) = [\omega(l) - 3\omega(l - \Delta\xi) + 3\omega(l - 2\Delta\xi) - \omega(l - 3\Delta\xi)] / \Delta\xi^3$ . Error in the estimation of the term  $\frac{EI}{M}\omega_{\xi\xi\xi}(l)$  arising from numerical measurements error may be merged with disturbance term  $d_2$ .

**Remark 4. (design novelty of observer).** Observer (21–26) features unique characteristics which render it an appropriate choice for application in the flexible manipulator. The design is based on the practical assumption of measurability of joint angle, which permits increased focus on obtaining distributed states. Hence, more intricate models for flexible systems can be considered for observer design, which can describe flexible systems with increased precision due to the existence of additional nonlinear terms—for example, system state and endpoint control-based terms featuring gravity effects in (13)—in comparison with homogeneous boundary conditions and linear deflection models [15, 37]. Incorporating additional estimation error dynamics between (11) and (21) would result in significantly more intricate calculations, which would have required the use of additional assumptions and simplifications to ensure the boundedness of corresponding terms. Additionally, the incorporation of decision variables in the proposed Lyapunov function conveniently ensures the feasibility of calculations. It has been demonstrated that (31) is solvable based on (52), which indicates that the solution for  $\alpha$  and  $\beta$  is obtainable at all moments according to the presented design. Condition (32) is subsequently attainable based on the selection of observer input  $u_{ob}$ .

**Remark 5. (calculating observer input).** Inequality (32) may be solved analytically or numerically using a number of methods. An analytical solution used for implementing the closed-loop system in this study is presented in Section 4. Numerical solutions—for example, using optimization solvers—can be selected for this purpose as well.

**Remark 6. (convergence based on observer input).** In proof of Theorem 1, convergence analysis of the observer was conducted in relation to the assigned CLF. This analysis is linked to input  $u_{ob}$  as  $\dot{V}_{ob} < -\sigma_{ob}V_{ob} - \epsilon_4 - u_{ob}z_1(l)$ , where  $\epsilon_4 = -\delta\alpha\beta\frac{EI}{\rho A}[-z_{\xi\xi\xi}(l) - 2z_{\xi\xi\xi}(0) + \frac{2}{l}z_{\xi}^2(l)] - \alpha^2\frac{EI}{\rho A}z_1z_{\xi\xi\xi}(l) - \dot{\theta}^2z_1(l)z(l) + \frac{EI}{M}z_1(l)z_{\xi\xi\xi}(l) + z(l)z_1(l)$ . Setting  $\epsilon_5 = [\epsilon_4 + u_{ob}z_1(l)]/V_{ob}$ , decay rate (A.25) is modified as  $\dot{V}_{ob} < -(\sigma_{ob} + \epsilon_5)V_{ob}$ .

**Remark 7. (observer simplification for implementation).** For implementation in real-time systems, the terms in the Lyapunov function corresponding to distributed states may be ignored to attain high calculation speed. The use of the modified Lyapunov function  $V_{ob} = V_s + \frac{1}{2}z^2(l) + \frac{1}{2}z_1^2(l)$  would ensure that endpoint displacement estimation  $\omega(l)$  is observed. Subsequently, displacement of the flexible link throughout its length  $\omega(\xi)$  is estimable based on modal analysis based on the estimation  $\hat{\omega}(\xi) = \sum_{i=1}^{m_\phi} \eta_i \phi_i(\xi)$  where  $m_\phi$  is the number of allocated basis functions  $\phi_i(\xi)$  (mode shapes).  $\phi_i(\xi)$  is estimable based on the boundary conditions of the system [18] and  $\hat{\omega}(l)$  is observable according to (21–26). Hence,  $\eta_i$  is estimable as  $\hat{\omega}(l) = \sum_{i=1}^{m_\phi} \eta_i \phi_i(l)$ . Distributed states throughout the length of the beam are then estimable as  $\hat{\omega}(\xi) = \sum_{i=1}^{m_\phi} \eta_i \phi_i(\xi)$  with high computation speed.

## 4 | Controller Design

This section details a novel boundary controller design for endpoint tracking of a flexible manipulator. This objective will be attained based on ensuring reference joint angle tracking, elimination of endpoint deflections, and mitigation of flexibility effects throughout the length of the flexible arm. A boundary control scheme will be designed considering the unavailability of distributed states describing link deflection and higher-order derivatives. On this basis, estimations of lateral deflections based on the distributed state observer presented in Section 3 will be incorporated into the controller design. Hence, modified dynamics (21–25) with respect to observer input  $u_{ob}$  calculated according to Theorem 1 are assigned to the controller in place of the original system dynamic (11–15). On this basis, the observer input  $u_{ob}$  ensures convergence of estimated distributed states to original system states, while the control input will guarantee the satisfaction of control objectives and stability of the closed-loop system.

To construct the controller in a convenient manner while considering interaction effects between various inputs and outputs, approximated governing equations of motion (21–25) are transformed to matrix form as follows. Initially, (22) is multiplied in  $\xi$  and then integrated over the length of the flexible beam.

$$\int_0^l \xi \hat{\omega}_t(\xi) d\xi = \dot{\theta}^2 \int_0^l \xi \hat{\omega}(\xi) d\xi - \frac{EI}{\rho A} \int_0^l \xi \hat{\omega}_{\xi\xi\xi\xi}(\xi) d\xi - \frac{1}{3} l^3 \dot{\theta} \quad (69)$$

Substituting (69) in (21), it follows that

$$\begin{aligned} & \left[ \hat{I}_m + \hat{M}l^2 + \hat{M}\hat{\omega}^2(l) + \hat{\rho}\hat{A} \int_0^l \hat{\omega}^2(\xi) d\xi - \frac{1}{3} \hat{\rho}\hat{A}l^3 \right] \ddot{\theta} + \hat{M}l\hat{\omega}_t(l) \\ & + 2\hat{M}\hat{\omega}(l)\hat{\omega}_t(l) + 2\hat{\rho}\hat{A} \int_0^l \hat{\omega}(\xi)\hat{\omega}_t(\xi) \dot{\theta} d\xi + \frac{1}{2} \hat{m}gl \cos \theta \\ & + \hat{M}gl \cos \theta - \hat{M}g\hat{\omega}(l) \sin \theta = \tau + F_b l + d_1 \end{aligned} \quad (70)$$

Then, based on (21) and (70), flexible system dynamics may be expressed using the new expression of the model as in (71–77) with boundary conditions (24) and (25).

$$\mathbf{M} \ddot{\mathbf{q}} + \mathbf{h} = \mathbf{B}(\mathbf{u} + \mathbf{d}) \quad (71)$$

$$\mathbf{M} = \begin{bmatrix} \hat{I}_h + \hat{M}l^2 + \hat{M}\hat{\omega}^2(l) + \hat{\rho}\hat{A} \int_0^l \hat{\omega}^2(\xi) d\xi, & \hat{M}l \\ & l, \\ & & 1 \end{bmatrix} \quad (72)$$

$$\mathbf{q} = \begin{bmatrix} \theta \\ \hat{\omega}(l) \end{bmatrix} \quad (73)$$

$$\mathbf{h} = \begin{bmatrix} 2\widehat{M}\hat{\omega}(l)\hat{\omega}_l(l)\dot{\theta} + 2\widehat{\rho}\widehat{A}\int_0^l \hat{\omega}(\xi)\hat{\omega}_l(\xi)\dot{\theta}d\xi + \frac{1}{2}\widehat{m}gl\cos\theta + \widehat{M}gl\cos\theta + \widehat{M}_g\hat{\omega}(l)\sin\theta \\ -\hat{\omega}(l)\dot{\theta}^2 + g\cos\theta - \widehat{s}_2\hat{\omega}_{\xi\xi\xi}(l) + u_{ob} \end{bmatrix} \quad (74)$$

$$\mathbf{B} = \begin{bmatrix} 1, & l \\ 0, & \frac{1}{M} \end{bmatrix} \quad (75)$$

$$\mathbf{u} = \begin{bmatrix} \tau \\ F_b \end{bmatrix} \quad (76)$$

$$\mathbf{d} = \begin{bmatrix} d_1 \\ d_2 \end{bmatrix} \quad (77)$$

It is noted that  $\mathbf{M} > 0$  as all elements of the matrix are positive and  $\det(\mathbf{M}) = I_h + M\hat{\omega}^2(l) + \rho A \int_0^l \hat{\omega}^2(\xi)d\xi > 0$ . In case  $I_h = 0$ , the modified stiffness matrix is positive-semidefinite, with the case of  $\det(\mathbf{M}) = 0$  corresponding to  $\hat{\omega}(\xi) = 0$  for  $\xi \in [0, l]$ .

Error dynamics for the controller is defined considering the objective of tracking reference joint angle signal  $\theta_r$  and elimination of endpoint deflection  $\hat{\omega}(l) = 0$ . Hence, the error dynamics for the controller are written as follows:

$$\dot{\mathbf{e}} = \mathbf{v} + \boldsymbol{\gamma}(\mathbf{u} + \mathbf{d}) \quad (78)$$

$$\mathbf{e} = \begin{bmatrix} \theta - \theta_r + \lambda_\theta(\theta - \theta_r) \\ \hat{\omega}(l) + \lambda_\omega\hat{\omega}(l) \end{bmatrix} \quad (79)$$

$$\mathbf{v} = -\mathbf{M}^{-1}\mathbf{h} + \begin{bmatrix} -\ddot{\theta}_r + \lambda_\theta(\dot{\theta} - \dot{\theta}_r) \\ \lambda_\omega\hat{\omega}_l(l) \end{bmatrix} \quad (80)$$

$$\boldsymbol{\gamma} = \mathbf{M}^{-1}\mathbf{B} \quad (81)$$

where  $|\lambda_\theta| > 1$  and  $|\lambda_\omega| > 1$  are control parameters. When obtaining the control law, the individual elements of (33) are addressed as follows:

$$\dot{e}_1 = v_1 + \gamma_{11}u_1 + \gamma_{12}u_2 + \hat{d}_1 \quad (82)$$

$$\dot{e}_2 = v_2 + \gamma_{21}u_1 + \gamma_{22}u_2 + \hat{d}_2 \quad (83)$$

where  $\hat{d}_1 = \gamma_{11}d_1 + \gamma_{12}d_2$  and  $\hat{d}_2 = \gamma_{21}d_1 + \gamma_{22}d_2$ , and the mentioned disturbance terms are bounded as  $d_1 \in \widehat{\mathcal{D}}_1$  and  $d_2 \in \widehat{\mathcal{D}}_2$ . The disturbance vector is defined as  $\widehat{\mathbf{d}} = [\widehat{d}_1, \widehat{d}_2]^T$ . The bounded modified disturbance vector is expressible as  $\widehat{\mathbf{d}} \in \widehat{\mathcal{D}} \triangleq \{\widehat{\mathbf{d}} \in \mathbb{R}^2 : \mathbf{d}_l < \widehat{\mathbf{d}} < \mathbf{d}_h\}$ .  $\mathbf{d}_l$  and  $\mathbf{d}_h$  express lower and upper disturbance bounds for uncertainty space  $\widehat{\mathcal{D}}$ .

**Theorem 2.** Control law (84) will ensure the satisfaction of control objectives and asymptotic stability of the closed-loop system.

$$\mathbf{u} = \mathcal{M}^{-1}\mathcal{R} \quad (84)$$

$\mathcal{M}$  and  $\mathcal{R}$  are functions of system dynamics, the corresponding Lyapunov function, and reference signals (exact expressions are listed in the proof).

*Proof.* The proof of Theorem 2 follows the steps below:

- i. Initially, we assign a CLF, demonstrating that it is non-increasing at all times.
- ii. The energy of the system is defined to be equal to the CLF, and based on the extended LaSalle's principle for infinite-dimensional systems, the stability of closed-loop systems is demonstrated.

To this end, CLF (B.1) is investigated to obtain a control law.

$$V = V_t + V_f \quad (85)$$

The terms  $V_t$  and  $V_f$  represent components of CLF corresponding to joint angle tracking and elimination of link-flexibility effects as well as that of endpoint deflections.

$$V_t = \frac{1}{2}e_1^2 \quad (86)$$

$$V_f = \frac{1}{2}e_2^2 + \frac{1}{2}c_f \int_0^l [\hat{\omega}_l^2(\xi) + \widehat{s}_1\hat{\omega}_{\xi\xi}^2(\xi)]d\xi \quad (87)$$

$c_f > 0$  is a decision variable dictating flexibility effects throughout the length of the link on control action. Each component of CLF is investigated on its own to obtain a more convenient control design while including interaction effects between various inputs and outputs. Afterward, combined information is used to obtain the control law.

Initially, the time derivative of  $V_t$  is analyzed based on (82) and (86).

$$\dot{V}_t = e_1\dot{e}_1 = e_1v_1 + e_1\gamma_{11}(u_1 + d_1) + e_1\gamma_{12}(u_2 + d_2) \quad (88)$$

It is assigned that

$$e_1v_1 + e_1\gamma_{11}u_1 + e_1\gamma_{12}u_2 = -\delta_1^2 - \xi_{d_1} \quad (89)$$

$$\xi_{d_1} = \text{Sup}_{\widehat{\mathcal{D}}}(e_1d_1 + e_1d_2) \quad (90)$$

$\delta_1 > \sqrt{|\xi_{d_1}|}$  is a control parameter. In case  $\widehat{\mathcal{D}}$  is a null space—that is, no disturbance term exists—it is assigned that  $\delta_1 > 0$ .

Next, the time derivative of  $V_f$  will be investigated based on (13), (83), and (87).

$$\begin{aligned} \dot{V}_f &= \int_0^l [\hat{\omega}_l(\xi)\hat{\omega}_l(\xi) + \widehat{s}_1\hat{\omega}_{\xi\xi}(\xi)\hat{\omega}_{l\xi\xi}(\xi)]d\xi \\ &+ e_2\dot{e}_2 = \int_0^l \left\{ [\hat{\omega}(\xi)\dot{\theta}^2 - \widehat{s}_1\hat{\omega}_{\xi\xi\xi\xi}(\xi) - \xi\ddot{\theta}]\hat{\omega}_l(\xi) \right\}d\xi \\ &+ \widehat{s}_1 \int_0^l \hat{\omega}_{\xi\xi\xi\xi}(\xi)\hat{\omega}_l(\xi)d\xi + e_2v_2 + e_2\gamma_{21}u_1 + e_2\gamma_{22}u_2 \end{aligned} \quad (91)$$

From (71), it holds that

$$\dot{\mathbf{q}} = \mathbf{v}_0 + \boldsymbol{\gamma}_0\mathbf{u} + \boldsymbol{\gamma}_0\widehat{\mathbf{d}} \quad (92)$$

$$\mathbf{v}_0 = -\mathbf{M}^{-1}\mathbf{h} \quad (93)$$

$$\boldsymbol{\gamma}_0 = \mathbf{M}^{-1}\mathbf{B} \quad (94)$$

Hence,  $\ddot{\theta}$  is expressed as follows:

$$\ddot{\theta} = v_{0_1} + \gamma_{0_{11}}u_1 + \gamma_{0_{12}}u_2 + \gamma_{0_{11}}d_1 + \gamma_{0_{12}}d_2 \quad (95)$$

After substituting (95) in (91), it is set that  $\dot{V}_f = -\delta_2^2$  where  $\delta_2 > \sqrt{|\xi_{d_2}|}$  is a control parameter. In the case of zero disturbance, it is assigned that  $\delta_2 > 0$ .

$$\begin{aligned} & \left[ e_2\gamma_{21} - \int_0^l \xi\gamma_{0_{11}}(\xi)\widehat{\omega}_l(\xi)d\xi \right] u_1 \\ & + \left[ e_2\gamma_{22} - \int_0^l \xi\gamma_{0_{12}}(\xi)\widehat{\omega}_l(\xi)d\xi \right] u_2 + \xi_0 = -\delta_2^2 - \xi_{d_2} \end{aligned} \quad (96)$$

$$\begin{aligned} \xi_0 = \int_0^l & \left\{ \left[ \widehat{\omega}(\xi)\dot{\theta}^2 - \widehat{s}_1\widehat{\omega}_{\xi\xi\xi\xi}(\xi) - \xi v_{0_1} \right] \widehat{\omega}_l(\xi) \right\} d\xi \\ & + \widehat{s}_1 \int_0^l \widehat{\omega}_{\xi\xi\xi\xi}(\xi)\widehat{\omega}_l(\xi)d\xi + e_2v_2 \end{aligned} \quad (97)$$

$$\begin{aligned} \xi_{d_2} = \text{Sup}_{\widehat{D}} & \left\{ \left[ e_2\gamma_{21} - \int_0^l \xi\gamma_{0_{11}}(\xi)\widehat{\omega}_l(\xi)d\xi \right] d_1 \right. \\ & \left. + \left[ e_2\gamma_{22} - \int_0^l \xi\gamma_{0_{12}}(\xi)\widehat{\omega}_l(\xi)d\xi \right] d_2 \right\} \end{aligned} \quad (98)$$

Equations (89) and (96) will be combined in matrix form as follows:

$$\mathbf{M}\mathbf{u} = \boldsymbol{\kappa} \quad (98)$$

$$\mathbf{M} = \begin{bmatrix} e_1\gamma_{11}, & e_1\gamma_{12} \\ e_2\gamma_{21} - \int_0^l \xi\gamma_{0_{11}}(\xi)d\xi, & e_2\gamma_{22} - \int_0^l \xi\gamma_{0_{11}}(\xi)d\xi \end{bmatrix} \quad (99)$$

$$\boldsymbol{\kappa} = \begin{bmatrix} -\delta_1^2 - e_1v_1 - \xi_{d_1} \\ -\delta_2^2 - \xi_0 - \xi_{d_2} \end{bmatrix} \quad (100)$$

Equation (98) is instantly solvable for  $\mathbf{u}$ , leading to (84), which completes the proof as it results in:

$$\dot{V} = -\delta_1^2 - \delta_2^2 \leq 0 \quad (101)$$

However, this does not prove that the closed system is stable. Conditions for the applicability of the extended LaSalle's principle for infinite-dimensional systems are investigated subsequently. To this end, closed-loop system dynamics are expressed in semi-linear form  $\dot{\mathbf{r}} = \mathcal{A}\mathbf{r} + f(\mathbf{r})$  (where  $\mathbf{r}$ ,  $\mathcal{A}$ , and  $f$  are specified later in the proof). Then, it is demonstrated that the following conditions are satisfied:

- i. Energy of the system has a negative time-derivative.
- ii.  $\mathcal{A}$  generates a continuous  $C_0$  semi-group of contraction.
- iii. Solution trajectories for  $\mathbf{r}$  are precompact.

To investigate conditions (i) and (ii), the dynamics of the closed-loop system have to be written in the form of a semi-linear differential equation. This is achievable by discretizing the displacement term  $\widehat{\omega}$  as follows:

$$\widehat{\omega}(\xi) = \sum_{i=1}^{m_\phi} \eta_i \phi_i(\xi) \quad (102)$$

where  $m_\phi$  is the number of allocated basis functions (mode shapes). The spaces corresponding to this mapping are defined as follows:

$$\phi_i(\xi) \in \mathcal{L}^2(0, L) \times \mathcal{H}^2(0, L) \quad (103)$$

$$\widehat{\omega}(\xi) \in \mathbb{R}^{m_\phi} \times \mathcal{L}^2(0, L) \times \mathcal{H}^2(0, L) \quad (104)$$

In which:

$$\mathcal{L}^2(0, L) = \left\{ f \mid \int_0^L |f|^2 < \infty \right\} \quad (105)$$

$$\mathcal{H}^k(0, L) = \left\{ f \mid f \in \mathcal{L}^2(0, L), \frac{\partial f}{\partial \xi} \in \mathcal{L}^2(0, L), \dots, \frac{\partial^k f}{\partial \xi^k} \in \mathcal{L}^2(0, L) \right\} \quad (106)$$

Spatial functions  $\phi_i(\xi)$  are uniquely determinable based on boundary conditions (24) and (25) and should satisfy orthogonality condition  $\int_0^l \phi_i(\xi)\phi_j(\xi)d\xi = 0$ .

Substituting (102) in (21–23) and noting that the spatial functions  $\phi_i(\xi)$  are orthogonal to each other—that is,  $\int_0^l \phi_i(\xi)\phi_j(\xi)d\xi = 0$ —closed-loop system dynamics are rewritten as follows:

$$\begin{aligned} & \left[ \widehat{I}_m + \widehat{M}l^2 + \widehat{M}\widehat{\omega}^2(l) + \widehat{\rho}\widehat{A} \sum_{i=1}^{\infty} \int_0^l \phi_i^2(\xi)d\xi \eta_i^2 \right] \ddot{\theta} \\ & + Ml\widehat{\omega}_l(l) + \sum_{i=1}^{\infty} \left[ \widehat{\rho}\widehat{A} \int_0^l \xi\phi_i(\xi)d\xi \right] \ddot{\eta}_i + 2\widehat{M}\widehat{\omega}(l)\widehat{\omega}_l(l) \\ & + 2\widehat{\rho}\widehat{A}\dot{\theta} \sum_{i=1}^{\infty} \int_0^l \phi_i^2 d\xi \eta_i \dot{\eta}_i + \frac{1}{2}\widehat{m}gl \cos \theta + \widehat{M}gl \cos \theta \\ & - \widehat{M}g\widehat{\omega}(l) \sin \theta = \tau + F_b l \end{aligned} \quad (107)$$

$$\sum_{i=1}^{\infty} \phi_i(\xi)\ddot{\eta}_i - \dot{\theta}^2 \sum_{i=1}^{\infty} \phi_i(\xi)\eta_i + \xi\ddot{\theta} + \widehat{s}_1 \sum_{i=1}^{\infty} \phi_{i\xi\xi\xi\xi}(\xi)\eta_i = 0 \quad (108)$$

Multiplying (107) in  $\phi_j(\xi)$ ,  $j = 1, \dots, \infty$ , considering orthogonality, and integrating over  $\xi \in [0, l]$  results in

$$\begin{aligned} & \int_0^l \phi_i^2(\xi)d\xi \ddot{\eta}_i - \dot{\theta}^2 \int_0^l \phi_i^2(\xi)d\xi \eta_i + \ddot{\theta} \int_0^l \xi\phi_i(\xi)d\xi \eta_i \\ & + \widehat{s}_1 \int_0^l \phi_i \phi_{i\xi\xi\xi\xi}(\xi)d\xi \eta_i = 0 \end{aligned} \quad (109)$$

Equations (23), (107), and (108) are combined in matrix form as follows:

$$\mathbf{M}_\phi \ddot{\mathbf{q}}_\phi + \mathbf{H}_\phi = \mathbf{B}_\phi \mathbf{u}_\phi \quad (110)$$

$$\mathbf{q}_\phi = [\theta, \widehat{\omega}(l), \eta_1, \eta_2, \dots]^T \quad (111)$$

$$M_{\phi_{11}} = \widehat{I}_m + \widehat{M}l^2 + \widehat{M}\widehat{\omega}^2(l) + \widehat{\rho}\widehat{A}\sum_{i=1}^{\infty}\int_0^l \phi_i^2(\xi)d\xi\eta_i^2 \quad (112)$$

$$M_{\phi_{12}} = \widehat{M}l \quad (113)$$

$$M_{\phi_{1(j=3,\dots,m_\phi+2)}} = \widehat{\rho}\widehat{A}\int_0^l \xi\phi_{j-2}(\xi)d\xi \quad (114)$$

$$M_{\phi_{21}} = l \quad (115)$$

$$M_{\phi_{22}} = 1 \quad (116)$$

$$M_{\phi_{2(j=3,\dots,m_\phi+2)}} = 0 \quad (117)$$

$$M_{\phi_{i1(i=3,\dots,m_\phi+2)}} = \int_0^l \xi\phi_{i-2}(\xi)d\xi\eta_i \quad (118)$$

$$M_{\phi_{i2(i=3,\dots,m_\phi+2)}} = 0 \quad (119)$$

$$M_{\phi_{ii(i=3,\dots,m_\phi+2)}} = \int_0^l \phi_{i-2}^2(\xi)d\xi \quad (120)$$

$$M_{\phi_{ij(i,j=3,\dots,m_\phi+2,i\neq j)}} = 0 \quad (121)$$

$$H_{\phi_1} = 2M\widehat{\omega}(l)\widehat{\omega}_l(l) + 2\widehat{\rho}\widehat{A}\widehat{\theta}\sum_{i=1}^{\infty}\int_0^l \phi_i^2 d\xi\eta_i\dot{\eta}_i + \frac{1}{2}\widehat{m}gl\cos\theta + \widehat{M}gl\cos\theta + \widehat{M}g\widehat{\omega}(l)\sin\theta \quad (122)$$

$$H_{\phi_2} = -\widehat{\omega}(l)\dot{\theta}^2 + g\cos\theta - \widehat{s}_2\widehat{\omega}_{\xi\xi\xi}(l) + u_{ob} \quad (123)$$

$$H_{\phi_{i(i>3)}} = -\dot{\theta}^2\int_0^l \phi_{i-2}^2(\xi)d\xi\eta_i + \widehat{s}_1\int_0^l \phi_{i-2}\phi_{i-2\xi\xi\xi}(\xi)d\xi\eta_i \quad (124)$$

$$B_\phi u_\phi = \left[ \tau + F_b l, \frac{1}{M}F_b, 0, 0, \dots, 0 \right]^T \quad (125)$$

Then, the nonlinear mapping describing closed-loop system dynamics is obtained as follows:

$$\dot{\mathbf{r}} = \mathcal{A}\mathbf{r} + f(\mathbf{r}) \quad (126)$$

$$\mathcal{S} = \mathbb{R}^{2m_\phi+4} \quad (127)$$

$$\mathbf{r} = [r_1, \dots, r_{2m_\phi+4}]^T, \mathbf{r}(0) \in \mathcal{S} \quad (128)$$

$$\begin{bmatrix} r_1, r_2, r_3, r_4, \dots, r_{2m_\phi+1}, r_{2m_\phi+4} \end{bmatrix}^T = \begin{bmatrix} \lambda_\theta\theta - \lambda_\theta\theta_r, \dot{\theta}, \lambda_\omega\widehat{\omega}(l), \lambda_\omega\widehat{\omega}(l), c_1\eta_1, c_1\dot{\eta}_1, \dots, c_{m_\phi}\eta_{m_\phi}, c_{m_\phi}\dot{\eta}_{m_\phi} \end{bmatrix}^T \quad (129)$$

$$\mathcal{A}\mathbf{r} = \begin{bmatrix} r_2 \\ M_{\phi_{11}}r_1 + \dots + M_{\phi_{1(m_\phi+2)}}r_{2m_\phi+1} \\ r_4 \\ \vdots \\ r_{2m_\phi+4} \\ M_{\phi_{(m_\phi+2)1}}r_1 + \dots + M_{\phi_{(m_\phi+2)(m_\phi+2)}}r_{2m_\phi+1} \end{bmatrix}, \mathcal{A}\mathbf{r} \in D(\mathcal{A}) = \mathcal{S} \quad (130)$$

$$f(\mathbf{r}) = \begin{bmatrix} 0 \\ -H_{\phi_1} + \tau + F_b l \\ 0 \\ -H_{\phi_2} + F_b \\ 0 \\ -H_{\phi_2} \\ \vdots \\ 0 \\ -H_{m_\phi+1} \end{bmatrix}, f(\mathbf{r}) \in \mathcal{S} \quad (131)$$

Nonlinear function  $f(\mathbf{r})$  is continuous and differentiable. The energy of the system (126) is assigned as  $E = V$  and is expressed in the form of an inner product as follows:

$$E = \|\mathbf{r}\|_{\mathcal{S}}^2 = \langle \mathbf{r}, \mathbf{r} \rangle_{\mathcal{S}} \quad (132)$$

$$E = \frac{1}{2}e_1^2 + \frac{1}{2}e_2^2 + \frac{1}{2}\sum_{i=1}^{m_\phi} c_{1i}\eta_i^2 + \frac{1}{2}\sum_{i=1}^{m_\phi} c_{2i}\eta_{it}^2 \quad (133)$$

$$c_{1i} = \int_0^l c_f \widehat{s}_1 \phi_{\xi\xi\xi}^2(\xi)d\xi + \phi_i^2(l) \quad (134)$$

$$c_{2i} = \int_0^l c_f \phi_i^2(\xi)d\xi \quad (135)$$

As  $E = V > 0$  and  $\dot{E} = \dot{V} \leq 0$ , condition (i) of the extended LaSalle's invariance principle is satisfied. Next, it is demonstrated that operator  $\mathcal{A}$  is dissipative. As  $\dot{E} \leq 0$ , it is expressible that

$$\dot{E} = \langle \mathbf{r}, \mathcal{A}\mathbf{r} + f(\mathbf{r}) \rangle_{\mathcal{S}} + \langle \mathcal{A}\mathbf{r} + f(\mathbf{r}), \mathbf{r} \rangle_{\mathcal{S}} = 2\langle \mathbf{r}, \mathcal{A}\mathbf{r} \rangle + \langle f, \mathbf{r} \rangle \leq 0 \quad (136)$$

$$\mathbf{f}_s = \langle \mathbf{r}, f(\mathbf{r}) \rangle + \langle f(\mathbf{r}), \mathbf{r} \rangle \quad (137)$$

Hence, the operator  $\mathcal{A}$  is dissipative. Based on the Lumer-Phillips theorem, (ii) holds if for some  $\lambda > 0$  range of  $\lambda I - \mathcal{A}$  is onto  $\mathcal{S}$ . For this, the operator  $\mathcal{A}$  has to be compact. As the kinetic energy of the system is expressible as  $\dot{q}_\phi^T M_\phi \dot{q}_\phi \geq 0$ ,  $M_\phi$  and  $\mathcal{A}$  are positive semi-definite. Hence,  $\mathcal{A}^{-1}$  exists and maps every bounded set on  $\mathcal{S}$  to a bounded set on  $\mathcal{S}$  and  $\mathcal{A}^{-1}$  is a compact operator that satisfies (ii). It follows that  $\mathcal{A}\mathbf{r} = \mathbf{g} \in \mathcal{S}$ , which has the unique solution  $\mathbf{r} = \mathcal{A}^{-1}\mathbf{g}$ . This also proves that the spectrum of  $\mathcal{A}$  consists of isolated eigenvalues. Hence,  $(\lambda I - \mathcal{A})^{-1} : \mathcal{S} \rightarrow \mathcal{S}$  is compact for any  $\lambda$  in a resolvent set of  $\mathcal{A}$ . Additionally, basis functions  $\phi_i(\xi)$  used in separation of variables are uniquely determinable based on the boundary conditions (23-25). The procedure to obtain  $\phi_i(\xi)$  is demonstrated by the authors in another work.

To investigate condition (iii), the following requirements for pre-compactness of solutions for (126) are studied [48].

- iii.a  $\mathcal{A}$  generates a bounded semigroup on  $S$ .
- iii.b  $f(\mathbf{r})$  is continuous and differentiable.
- iii.c For every  $t = t_1 > 0$  the following inequality holds:

$$\mathbf{r}(t) = T(t)\mathbf{r}(0) + \int_0^t T(t-\tau)f[\mathbf{r}(\tau)]d\tau \quad (138)$$

- iii.d  $f(\mathbf{r})$  is bounded as  $\text{Sup}_{t>0} \left\| \int_0^t T(t-\tau)f[\mathbf{r}(\tau)]dt \right\| < \infty$  where  $T(t)$  is a  $C_0$  semi-group.

The conditions (iii.a) and (iii.b) already hold based on the previous steps of the proof. (iii.c) is verified by assigning the mapping  $T(t) = e^{\mathcal{A}t}$ . As the weak solution of (126) for  $\mathbf{r}$  should satisfy Duhamel's formula, it holds that:

$$\mathbf{r}(t) = e^{\mathcal{A}t}\mathbf{r}(0) + \int_0^t e^{\mathcal{A}(t-\tau)}f[\mathbf{r}(\tau)]d\tau \quad (139)$$

Hence, (iii.c) is verified. To investigate condition (iii.d), energy balance for time  $t$  is studied based on (101) with respect to initial energy balance.

$$E(t) = E(0) + \int_0^t [\delta_1^2(\tau) + \delta_2^2(\tau)]d\tau \quad (140)$$

Hence, from the definition (132), it is obtained that  $\|\mathbf{r}(t)\|_S^2 = E(t) \leq E(0)$ . Substituting (139) for  $\mathbf{r}(t)$ , it follows that  $\mathbf{r}(t)$  is bounded as  $\|\mathbf{r}(t)\|_S^2 = \left\| e^{\mathcal{A}t}\mathbf{r}(0) + \int_0^t e^{\mathcal{A}(t-\tau)}f[\mathbf{r}(\tau)]d\tau \right\|_S^2 \leq E(0) < \infty$ . Hence, condition (iii.d) is verified. This also implies that the nonlinear term  $\int_0^t f[\mathbf{r}(\tau)]d\tau < \infty$ . Therefore, the pre-compactness of solution trajectories is validated, which satisfies condition (iii) of the extended LaSalle's invariance principle.

It has been demonstrated that all conditions of LaSalle's invariance principle are validated, and  $V$  converges to zero. Then, from (85), it follows that  $e_1, e_2, \hat{\omega}_l(\xi)$ , and  $\hat{\omega}_{\xi\xi}(\xi)$  decay to zero. Hence, based on (34),  $\theta \rightarrow \theta_r$  and  $\hat{\omega}(l) \rightarrow 0$ . Furthermore, as  $\hat{\omega}(0) = \hat{\omega}_\xi(0) = \hat{\omega}_{\xi\xi}(l) = 0$  and  $\hat{\omega}(l) \rightarrow 0$ , it follows that  $\hat{\omega}(\xi) \rightarrow 0$ . Finally, based on (A.25), it was established in the proof of Theorem 1 that  $\int_0^l z^2 d\xi$  is bounded and decays to zero. Hence,  $z(\xi) \rightarrow 0$  and  $\hat{\omega}(\xi) \rightarrow \omega(\xi) \rightarrow 0$ . This results in satisfaction with all control objectives and completes the proof.

**Remark 8. (incorporation of distributed state observer).** As seen from the proof of Theorem 2, the displacement values throughout the length of flexible beam  $\omega(\xi)$  and corresponding time-derivatives are required to obtain precise control action. Hence, the values of distributed states for  $\xi \in (0, l)$  are needed, while in practical applications commonly only boundary state feedback  $\omega(l)$  is available. This highlights the need for the use of an appropriate estimation scheme in control design.

**Remark 9. (orthogonality of spatial functions).** Functions  $\phi_i(\xi)$  used in separation-of-variables method must satisfy boundary conditions (23–25) and orthogonality condition  $\int_0^l \phi_i(\xi)\phi_j(\xi)d\xi = 0$ . A standard implementation method [18] involves assigning  $\phi_i(\xi) = c_{1i}(\cos \beta_i \xi + \cosh \beta_i \xi) + c_{2i}(\cos \beta_i \xi - \cosh \beta_i \xi) + c_{3i}(\sin \beta_i \xi + \sinh \beta_i \xi) + c_{4i}(\sin \beta_i \xi - \sinh \beta_i \xi)$  and subsequently calculating coefficients  $c_{1i}, c_{2i}, c_{3i}$ , and  $c_{4i}$  such that boundary conditions and orthogonality condition are satisfied [6].

**Remark 10. (required measurements).** Measurements of  $\theta, \dot{\theta}, \omega(l), \omega_l(l)$ , and  $\omega_{\xi\xi\xi}(l)$  should be obtained online in order to implement the control systems.

**Remark 11. (control parameters).** The control parameters that are assigned to the controller and observer are summarized in Table 1.

Decision variables  $\alpha$  and  $\beta$  are selected according to (31) such that the feasibility of the Lyapunov function is ensured. Control parameter  $\delta$  and its upper bound  $p$  are assigned such that decay of the Lyapunov function can be ensured based on (52). Similarly,  $\lambda_\theta$  and  $\lambda_\omega$  indicate the rate of convergence to reference values. Higher magnitudes would prioritize faster convergence, respectively, to desired joint angle signal and elimination of undesired deflections at the cost of potentially increased inputs and spikes in corresponding input signals.  $c_f$  indicates the significance of alleviating deflection effects throughout the length of the flexible beam in control objectives. In cases where only endpoint control is desired,  $c_f = 0$  is assigned for convenience.  $\delta_1$  and  $\delta_2$  indicate the decay of Lyapunov function components corresponding to  $e_1$  and  $\omega(\xi)$  for  $\xi \in [0, l]$ , which should be assigned such that realizable input values are attained. Based on (100), it can be assigned such that  $\delta_1$  and  $\delta_2$  attain values corresponding to  $\sqrt{|e_1 v_1|}$  and  $\sqrt{|\xi_0|}$ , respectively.

**TABLE 1** | Control and observer parameters.

Parameter	Definition	Parameter	Definition
$\alpha$	Decision variable for the observer Lyapunov function	$c_f$	Control parameter for link flexibility effects in the controller
$\beta$	Decision variable for the observer Lyapunov function	$\delta_1$	Control parameter corresponding to $\dot{V}_l$ for the controller
$\lambda_\theta, \lambda_\omega$	Control parameters for joint angle tracking error and endpoint deflection	$\delta_2$	Control parameter corresponding to $\dot{V}_f$ for the controller
$\delta$	Decision variable for the design of the Lyapunov function $V_{ob}$	$p$	Upper bound for $\delta$

**Remark 12. (controller design).** The proposed control strategy is fundamentally different from existing research work that deals with simultaneous robot joint-angle control and elimination of flexible link displacement, in that it is based on the consideration of the two control objectives in a MIMO framework instead of the common strategy of investigating a single Lyapunov function [5, 28, 29]. By ensuring the decay of components of the overall Lyapunov function  $V_l$  and  $V_f$  corresponding to joint angle tracking and elimination of vibration effects, this approach results in the calculation of control law in a succinct and convenient manner, which is also easily extendable to other systems. At the same time, effects of high-speed vibration effects are included in joint angle control as interaction effects in corresponding terms in mathematical model (71) are directly incorporated in the calculation of control law (84), which is different from perturbation-based strategies that divide the overall system into slow and fast subsystems [37].

**Remark 13. (controller downsides).** A potential downside of the controller is the occurrence of the chattering effect in control law (84). This is caused because controller assigns control input such that  $V$  converges to zero, potentially resulting in the occurrence of sign function terms in the calculations due to the division of squared error terms in error values themselves. If overcoming chattering effects is desired, error magnitudes in which input chattering begins to occur may be analytically or numerically obtained as  $|e_i| < \zeta_i$  and then for values of error smaller than  $\zeta_i$ , error values would be replaced by  $\zeta_i$ . Appropriate modifications of  $e_i$  for chattering alleviation—for example, tangent hyperbolic functions [49, 50]—may be assigned as well. While chattering effects would be alleviated or eliminated in this approach, this would result in boundedness of the Lyapunov function and tracking error in the corresponding region instead of convergence to zero in the absence of uncertainty terms. Hence, conveniently realizable input would be obtained at the cost of reduced control precision [51, 52].

**Remark 14. (controller simplification for implementation).** Similar to the Remark for implementation of the partial-state observer, distributed terms in the assigned Lyapunov function may be ignored as  $V = \frac{1}{2}e_1^2 + \frac{1}{2}e_2^2$ , which significantly improves the speed of numerical calculations, at the cost of reduced capability of mitigating deflection effects throughout the length of the beam. In this case, joint angle tracking and endpoint deflection mitigation are attained. In practice, this often leads to a reduction of flexibility effects throughout the length of the flexible link.

**Algorithm 1.** *The procedure for constructing a complete feedback loop featuring a distributed state observer and corresponding PDE controller is described in Table 2. The table expresses the implementation of the presented scheme in pseudo-code form for numerical or experimental implementation. The procedure is described at  $t = nT$  where  $n$  is an integer and  $T$  is the sampling time of implementation.*

The block diagram of the closed-loop system presenting an overview of the flexible mechanism, estimation scheme, and control algorithm in relation to each other is presented in Figure 2.

**TABLE 2** | Implementation of model-based PDE partial-state observation and control (MPOC).

---

```

// initial configuration
i. input  $x_{l,r}, y_{l,r}$ 
ii. input  $\lambda_\theta, \lambda_\omega, c_f$ 
iii. input  $s_l, s_h$ 
// Distributed-states observer: sample n
iv. calculate  $\theta_r$ 
v. record  $\theta, \dot{\theta}, \omega(l), \omega_t(l), \omega_{\xi\xi\xi}(l)$ 
vi. assign  $\alpha, \beta, p$ , and  $\delta$  (31)
vii. solve (32) for  $u_{ob}$ 
viii. exert  $u_{ob}$  to (21–26)
ix. solve (21–26) for  $\hat{\omega}(\xi)$ 
// PDE-based controller: sample n
x. calculate  $e$  (34)
xi. calculate  $\nu, \nu_0, \gamma, \gamma_0$  (80, 92)
xii. calculate  $\xi_0$  (96)
xiii. input  $d_l, d_h$ 
xiv. input  $\delta_1, \delta_2$  (100)
xv. calculate  $\mathcal{M}, \mathcal{R}$  (99, 100)
xvi. solve (84) for  $\underline{u}$  (84)
// Implementation of control action
xvii. exert  $\underline{u}$  to () (21–25)
xviii.  $n = n + 1$ 
xix. goto (iii)

```

---

**Remark 15. (stability of closed-loop system).** The closed-loop system depicted in Figure 2, featuring a partial-state observer and MPOC controller, is stable, as the compound Lyapunov function of the closed-loop system  $V_{cl} \triangleq V + V_{ob}$  retains characteristics of  $V_{ob}$  and  $V$  previously demonstrated in the proof of Theorem 1 and the proof of Theorem 2, respectively.

## 5 | Results and Analysis

In this section, the performance of the proposed distributed-state observer and PDE-based controller is investigated using numerical simulations. The mechanical and geometric properties of the simulated system as well as the fixed decision variables used in the estimation and control scheme are described in Table 3.

Control and estimation efficiency are investigated for tracking of desired joint angle trajectory  $\theta_r = a_r \cos \omega_r [rad]$  with  $a_r = 0.62 [rad]$  and  $\omega_r = 0.9 \pi [rad/s]$ . Combined with elimination of undesired deflection  $\omega(\xi)$  for  $\xi \in [0, l]$ , this results in tracking of associated cartesian position reference  $(x_{l,r}, y_{l,r}) = (l \cos \theta_r [m], l \sin \theta_r [m])$  which satisfies all control objectives previously indicated in Remark 1.  $\alpha, \beta$ , and  $\delta$  are assigned online

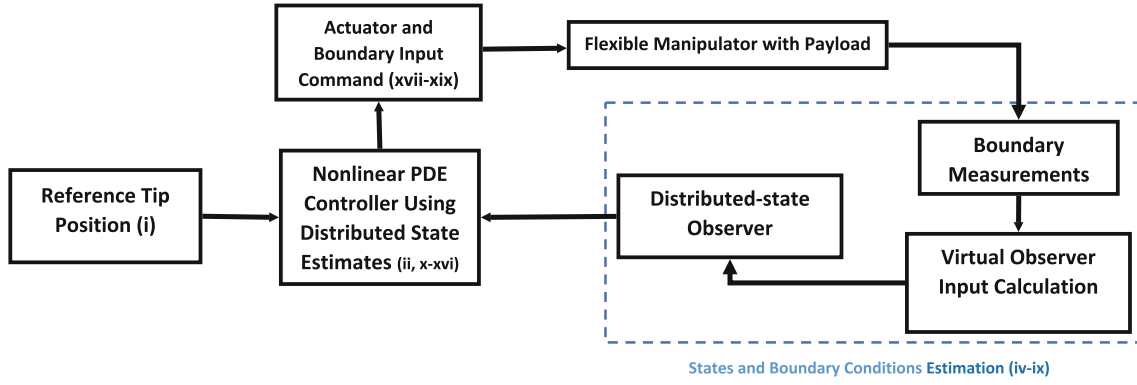


FIGURE 2 | Block diagram of the closed-loop system.

TABLE 3 | Mechanical, geometric, and numerical properties of closed-loop systems.

Parameter	Value	Parameter	Value
$\rho A$	2.34 [kg/m]	$c_f$	0.05
$EI$	$4.5e3$ [N.m <sup>2</sup> ]	$\lambda_\theta, \lambda_\omega$	5
$l$	1.00 [m]	$I_h$	0.01 [kg.m <sup>3</sup> ]
$M$	2.00 [kg]	$g$	9.81 [m/s <sup>2</sup> ]

such that they satisfy the corresponding feasibility conditions expressed in Sections 3 and 4. The issue of uncertainty in boundary conditions in real-world implementation will also be considered by assigning a faulty initial measurement of  $\hat{\omega}(l) = 0.10$  [m] with respect to the assigned factual value of  $\omega(l) = 0.00$  [m] for the original system. As described in Table 2, several decision variables are assigned online in order to ensure the feasibility of calculations. It is set that  $\delta_1 = 0.95\sqrt{|e_1 v_1|}$  and  $\delta_2 = 0.9\sqrt{|\xi_0|}$ . According to (23), for the feasibility of observer calculations and depending on the value of  $\theta$ , it is set that  $p = 2.01 \max(\theta, 1)$  and  $\delta$  is selected in the admissible bound  $(0, p)$  as  $\delta = \frac{1}{2}$ . Control parameters  $\alpha$  and  $\beta$  are calculated online according to (23) depending on the state configuration of the system. This is conducted by calculating the roots of the second-order equation for  $c$  based on (A.11) and (A.12) as  $c^2 - pc + \theta^2 = 0$  for  $|\theta| > 1$  and for  $c^2 - p\theta^2 c + \theta^2 = 0$  for  $|\theta| < 1$ . Then,  $c$  is set at the middle of the admissible bound between the roots. Afterward, setting  $\beta = \alpha c$  in (23), (23) is instantly solved online for  $\alpha$ . Initially, no parametric uncertainty or external disturbance is considered in the simulations, whose effects will be investigated subsequently.

The response of the closed-loop system for the aforementioned configuration is described in Figures 3–5.

Figure 3 indicates the convergence of the closed-loop system response to the associated reference signals, which have been guaranteed using stability-proved PDE-based control analysis. As described in Figure 4, the use of the proposed boundary control scheme has resulted in the mitigation of endpoint deflection of the beam. Additionally, Figure 4a indicates the convergence of  $\hat{\omega}(l)$  to actual measurement  $\omega(l)$  in finite time. Exact convergence to zero would necessitate that the convergence speed of the controller would exceed the rate of change in the system

states, which may not necessarily be realizable based on input constraints, uncertainty terms, or limitations of numerical calculations. In Figure 4b, observer input is described, which is exerted on the observer model (21–26). Similarly, the deflection of the flexible beam throughout its length is eliminated, as observed in Figure 4c. The input torque of the manipulator as well as the boundary input force calculated for the current control configuration are depicted in Figure 5 and retain bounded values throughout the operations.

In Table 4, the effects of the control parameter  $\lambda_\theta$ ,  $\lambda_\omega$ , and  $c_f$  on average tracking error magnitude (ATEM) of  $e_1$  corresponding to joint angle and the effect on the magnitude of endpoint displacement  $\hat{\omega}(l)$  in the interval between  $t = 3.0$  [s] and  $t = 5.0$  [s], as well as maximum input magnitude (MIM) of input torque  $\tau$  and boundary input force  $F_b$  in the aforementioned interval, are investigated. This table indicates that control objectives are attained with all assigned configurations. However, higher magnitudes of  $\lambda_\theta$  and  $\lambda_\omega$  correspond to smaller tracking errors in the steady-state of the system response, as the control system prioritizes faster tracking of changes in the reference signal. Control variable  $c_f$  assigns the significance of mitigation of flexibility effects. Higher values prioritize mitigation of deflection effects at the cost of reduced joint angle tracking precision. Control input values retain boundedness in all of the aforementioned configurations.

In Figure 6, the more pronounced effect of control parameters  $\delta_1$  and  $\delta_2$  system response is investigated. This is conducted based on an analysis of their cumulative effect in the term  $-\delta_1^2 - \delta_2^2$ . To this end, it has been assigned that  $\delta_1 = c_\delta \sqrt{|e_1 v_1|}$  and  $\delta_2 = c_\delta \sqrt{|\xi_0|}$ , where  $c_\delta$  is the corresponding design variable. Figure 6 depicts the effect of  $c_\delta$  on the time required for convergence of  $\theta$  to  $\theta_r$ , by recording the time  $t_c$  when error value  $|e_1(t_c)| = 0.05|e_1(t=0)|$  is recorded, as well as the effect of  $c_\delta$  on maximum input torque magnitude in the interval  $(0, t_c)$ . As observed in Figure 6, higher values of  $c_\delta$  would force a faster reduction in the Lyapunov function, which corresponds to a smaller convergence time. However, larger inputs are generated to attain this requirement.

In Figure 7, the boundedness and performance of the closed-loop system response in the presence of deviations from the nominal model featuring external disturbance and measurement noise are expressed. To this end, noisy state measurements are considered

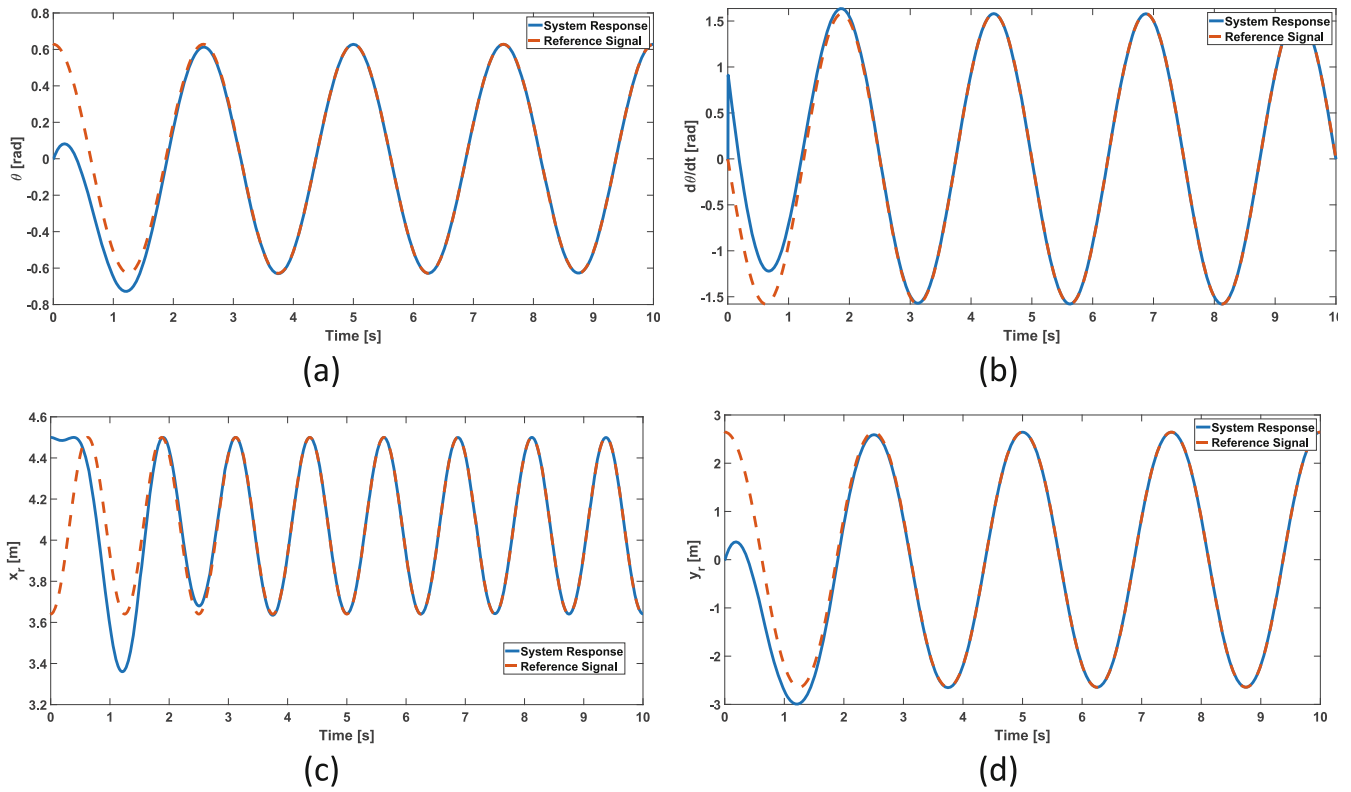


**FIGURE 3** | Tracking the performance of the controller: (a) joint angle; (b) joint velocity; (c) endpoint horizontal position; (d) endpoint vertical position.

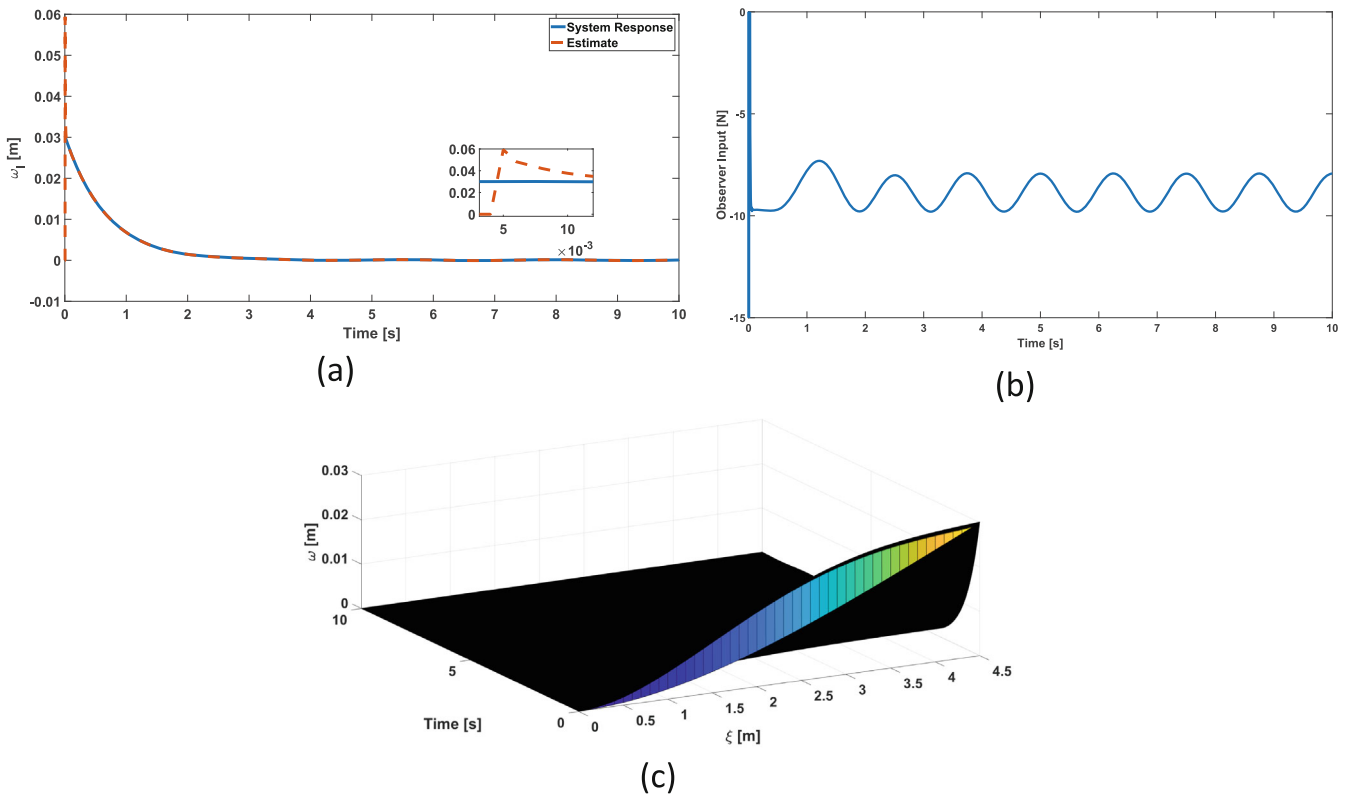


**FIGURE 4** | Deflection of the flexible beam and its estimate: (a) endpoint deflection and its estimate when applying boundary input; (b) observer input; (c) displacement of the flexible beam throughout its length.

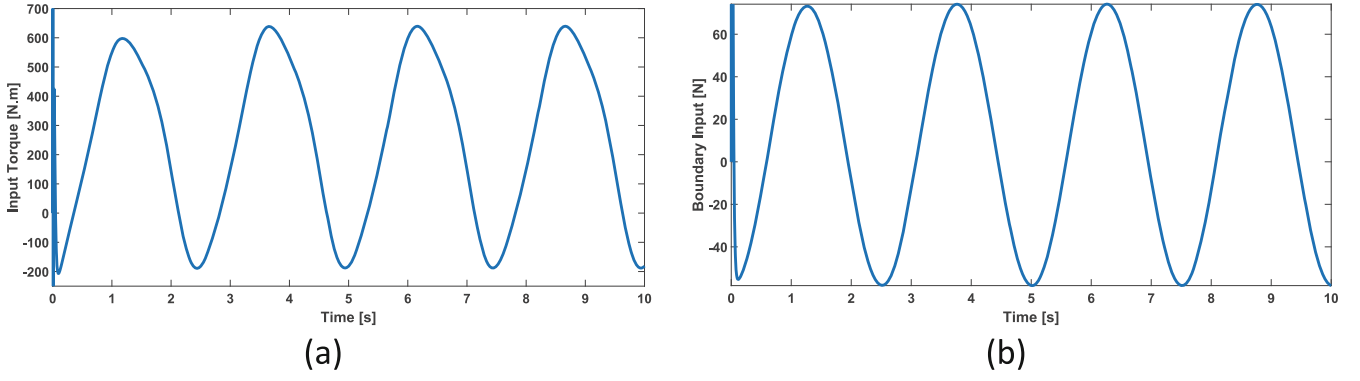


FIGURE 5 | Control input signals: (a) input torque; (b) boundary input force.

TABLE 4 | Numerical analysis of effects of the control parameter  $\lambda_\theta$ ,  $\lambda_\omega$ , and  $\beta$ .

Control parameter		$\lambda_\theta = \lambda_\omega$ (with $c_f = 0.05$ )				$c_f$ (with $\lambda_\theta = \lambda_\omega = 5$ )			
Error measure	Characteristic	3.0	4.0	5.0	6.0	0.03	0.04	0.05	0.06
ATEM	Joint angle	0.0674	0.0457	0.0312	0.021	0.0275	0.0292	0.0312	0.0675
	Endpoint displacement	0.0092	0.0062	0.0043	0.0029	0.0073	0.0058	0.0043	0.0030
MIM	Input torque	547.33	547.08	546.92	546.95	546.31	547.23	546.92	545.07
	Boundary input force	86.22	86.17	86.15	86.16	86.18	86.18	86.15	86.08

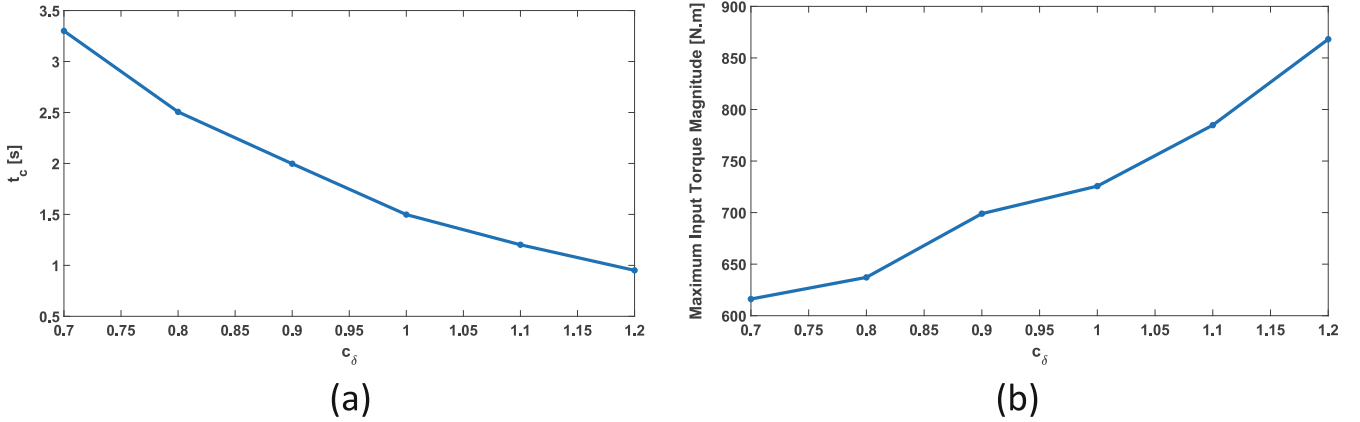
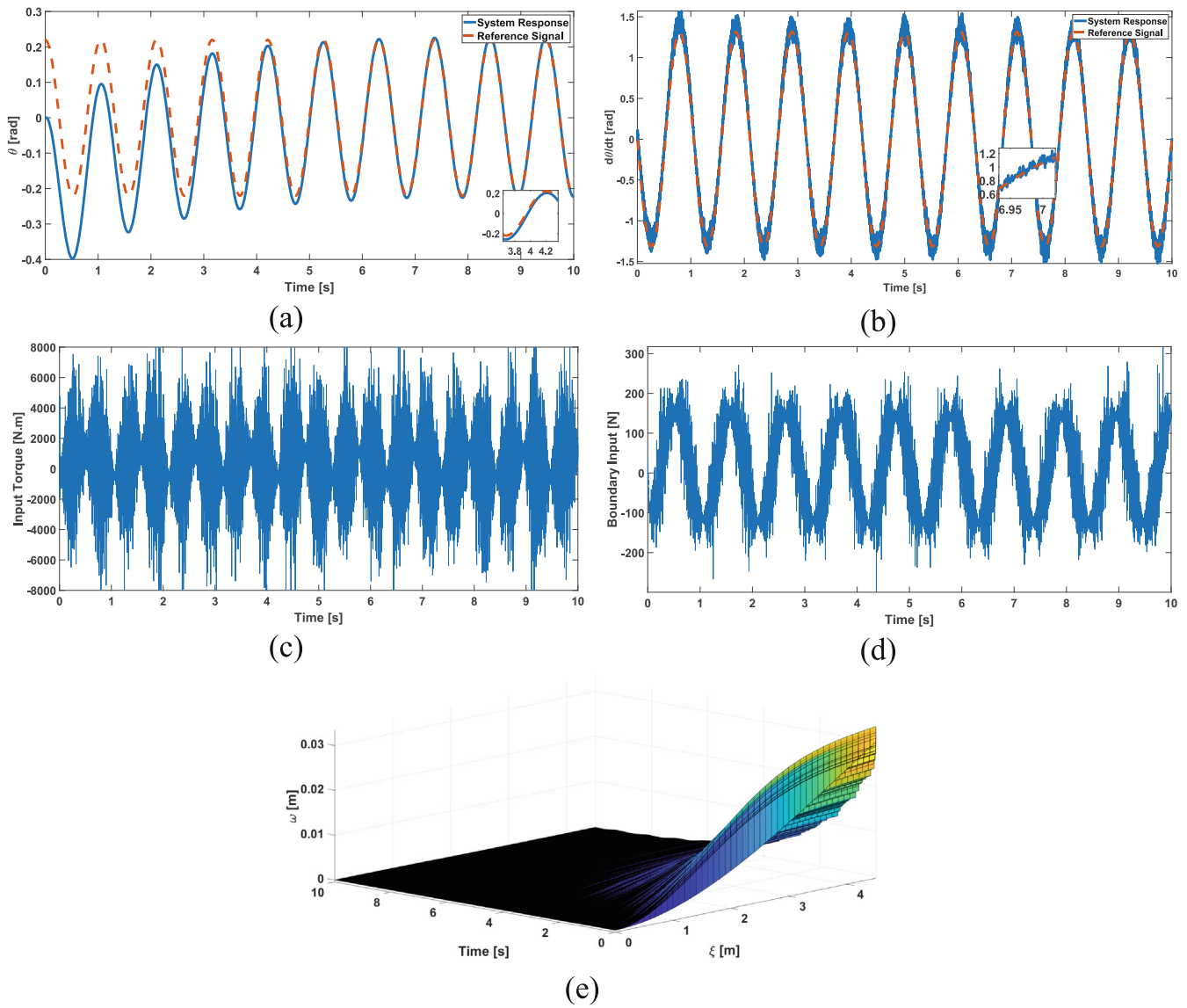


FIGURE 6 | Effect of  $c_\delta$  on convergence time and maximum input torque magnitude: (a) convergence time; (b) input torque magnitude.

in the calculation of control input as  $\hat{q}_i = [0.95 + 0.1N(0, 1)]q_i$ , additive disturbance equal to  $0.02 \mathbf{u}$ . As external noise is more relevant in higher-frequency vibrations, a higher-frequency desired signal  $\theta_r$  with  $a_r = 0.22[rad]$  and  $\omega_r = 1.9 \pi[rad/s]$  is considered, which excites two natural frequencies. Hence, larger inputs are observed in this example, alongside measurement noise effects. System response and inputs retain bounded values, and control objectives of tracking of desired signal  $\theta_r$  as well as mitigation of deflection effects are achieved. The deflection profile of the flexible beam depicted in Figure 7e indicates excitation of two natural frequencies, in contrast with Figure 4c, where excitation of only the first natural frequency was observed. As depicted in Figure 8, the closed-loop system maintains a bounded response in all investigated cases and successfully mitigates joint angle tracking error and endpoint displacement despite the presence of additive parametric uncertainty. As expected, higher error values

were observed in cases where higher values of parametric uncertainty were considered. This corresponds to an increased initial error for systems with larger parametric uncertainty and is eliminated over time.

Figure 9 features an analysis of control performance with respect to the potential-differential-strain feedback controller (PDS) in the newly added. PDS inputs are assigned as  $\tau = -k_{p,\theta}e_1 - k_{d,\theta}\dot{e}_1 - k_{i,\theta} \int e_1 dt$  and  $u = -k_{p,\omega}\omega(l) - k_{d,\omega}\dot{\omega}(l) - k_{s,\omega}\omega_{\xi\xi\xi}(l)$ . Based on the manipulator configuration, for the PDS controller to demonstrate satisfactory performance, a high-gain approach must be attained. Controller gains were set as  $k_{p,\theta} = k_{p,\omega} = 50000$ ,  $k_{d,\theta} = k_{d,\omega} = 2000$ , and  $k_{s,\omega} = 5$ . The results of the comparisons are depicted in Figure 8. As indicated, the main difference is that the MPOC scheme proposed in this study ensures gradual mitigation of joint angle tracking error and endpoint displacement,



**FIGURE 7** | Performance of the closed-loop system in the presence of measurement noise and external disturbance: (a) joint angle; (b) joint angular velocity; (c) input torque; (d) boundary input force; (e) displacement of the flexible beam.

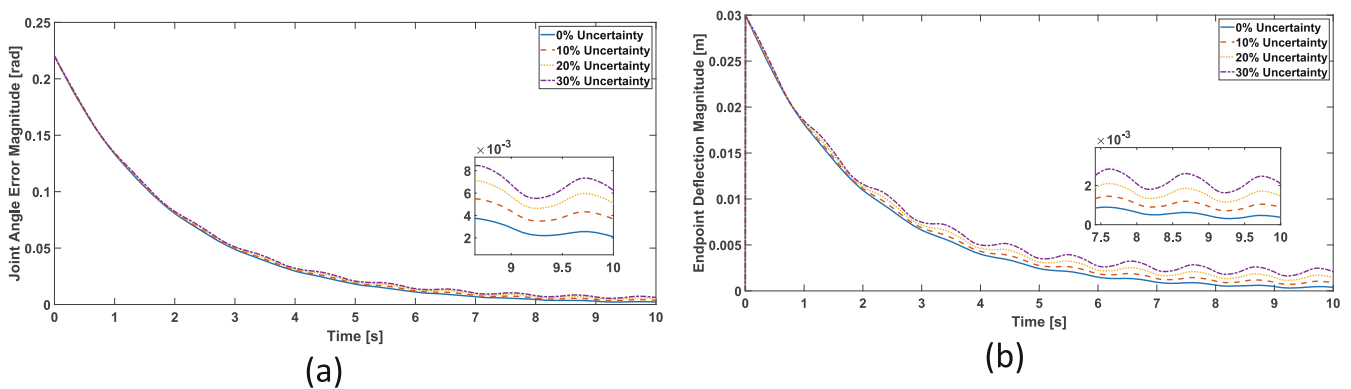


**FIGURE 8** | Error analysis based on parametric uncertainty percentage: (a) joint angle tracking error magnitude; (b) endpoint deflection.

as indicated by stability analysis, while the PDS controller maintains boundedness of states in an area around the origin, as the variable dynamic terms and coupling effects are not

considered. Specific modifications for the PDS controller may be conducted to include the aforementioned effects. Furthermore, the performance of the PDS controller is highly dependent on

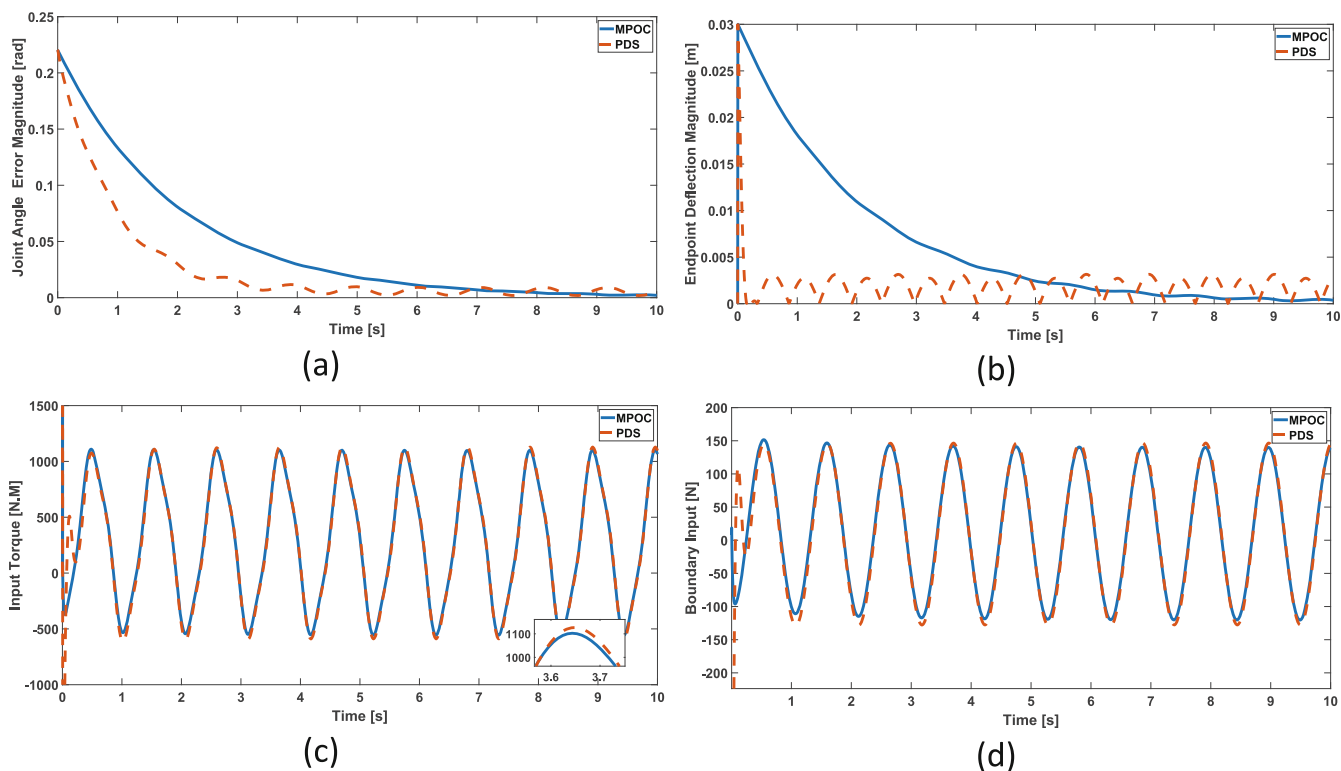


**FIGURE 9** | Comparative analysis of MPOC and PDS controllers: (a) joint angle error magnitude; (b) endpoint deflection magnitude; (c) input torque; (d) boundary input force.

controller gain, and the selection of unsuitable gains may result in instability of the system in case prior stability analysis is not conducted. In MPOC, any control parameter selected within the feasible region would maintain boundedness and stability and would only affect control performance. The potential drawback of the MPOC controller is the complexity of model-based design and distributed state measurement, which are not required in the PDS controller. Additionally, the high gains required for attaining acceptable performance in the PDS controller potentially result in high sensitivity to measurement noise due to their direct and magnified effect on control input, which is mitigated in the MPOC controller.

## 6 | Conclusions

This paper details the design of novel schemes for distributed state estimation and precise endpoint control of flexible manipulators using realistic PDE-based calculations. No simplifications, such as assumed modes or finite-element analysis, were considered at any stage of the closed-loop design, and the PDE model of the dynamic system was incorporated at all stages. Furthermore, it was acknowledged that the distributed states describing the configuration of a flexible manipulator may not be precisely known, as the boundary configuration of a mechanism may not be readily measurable in many applications. To address these issues, we proposed a new partial state observer for efficiently estimating flexible dynamics and introduced a corresponding boundary controller for joint angle tracking and elimination of endpoint deflection. Rigorous stability analysis based on the extended LaSalle's invariance principle for infinite-dimensional

systems demonstrated that all control objectives were achieved. The controller design allows for the convenient calculation of inputs to satisfy multiple objectives while directly incorporating interaction effects in the control calculations and featuring the capability to adapt to parametric model uncertainty. Numerical simulations have demonstrated the precision and efficiency of the proposed methods. Future research opportunities include obtaining analytical solutions for non-homogeneous PDE models, extending the research to robotic systems with a higher number of robotic arms, considering shear deformation effects in Timoshenko beams, including longitudinal deflection in the dynamic model, and investigating endpoint tracking problems within an optimal control framework.

### Acknowledgments

This work was supported by the Academy of Finland under the project "Nonlinear PDE-model-based control of flexible manipulators" (Grant No. 355664).

### Conflicts of Interest

The authors declare no conflicts of interest.

### Data Availability Statement

The data that support the findings of this study are available from the corresponding author upon reasonable request.

### References

1. H. Gao, Z. Yu, J. Hu, and C. Sun, "Adaptive Composite Learning Control of a Flexible Two-Link Manipulator With Unknown Spatiotemporally

- Varying Disturbance,” *International Journal of Robust and Nonlinear Control* 34, no. 12 (2024): 7764–7785, <https://doi.org/10.1002/rnc.7362>.
2. R. Mohsenipour and G. Liu, “Tip Position Control of Flexible Single-Link Manipulators in the Frequency Domain Without Model Reduction,” *International Journal of Robust and Nonlinear Control* 34, no. 6 (2024): 3994–4013, <https://doi.org/10.1002/rnc.7174>.
3. R. H. Lei and L. Chen, “Finite-Time Tracking Control and Vibration Suppression Based on the Concept of Virtual Control Force for Flexible Two-Link Space Robot,” *Defence Technology* 17, no. 3 (2021): 874–883, <https://doi.org/10.1016/j.dt.2020.04.013>.
4. W. Zhu, Q. Zong, L. Dou, B. Tian, and W. Liu, “Finite-Time Attitude Tracking Control and Vibration Suppression for Flexible Spacecraft,” *International Journal of Robust and Nonlinear Control* 31, no. 7 (2021): 2674–2689, <https://doi.org/10.1002/rnc.5420>.
5. F. Cao and J. Liu, “Boundary Control for a Constrained Two-Link Rigid–Flexible Manipulator With Prescribed Performance,” *International Journal of Control* 91, no. 5 (2018): 1091–1103, <https://doi.org/10.1080/00207179.2017.1305513>.
6. S. Yaqubi, S. M. Tahamipour-Z, and J. Mattila, “Semi-Analytical Design of PDE Endpoint Controller for Flexible Manipulator With Non-Homogenous Boundary Conditions,” *IEEE Transactions on Automation Science and Engineering* 21, no. 4 (2024): 7257–7274, <https://doi.org/10.1109/TASE.2023.3340332>.
7. I. H. Herron and M. R. Foster, *Partial Differential Equations in Fluid Dynamics* (Cambridge University Press, 2008), <https://doi.org/10.1017/CBO9780511754654>.
8. G. S. Carlo, *Electromagnetic Waves* (CRC Press, 2017), <https://doi.org/10.4324/9781420009545>.
9. M. Athanasopoulos, H. Ugail, and G. G. Castro, “Parametric Design of Aircraft Geometry Using Partial Differential Equations,” *Advances in Engineering Software* 40, no. 7 (2009): 479–486, <https://doi.org/10.1016/j.advengsoft.2008.08.001>.
10. Y. Achdou, F. J. Buera, J. M. Lasry, P. L. Lions, and B. Moll, “Partial Differential Equation Models in Macroeconomics,” *Philosophical Transactions of the Royal Society A: Mathematical, Physical and Engineering Sciences* 372, no. 2028 (2014): 20130397, <https://doi.org/10.1098/rsta.2013.0397>.
11. M. J. Simpson, R. J. Murphy, and O. J. Maclaren, “Modelling Count Data With Partial Differential Equation Models in Biology,” *Journal of Theoretical Biology* 580 (2024): 111732, <https://doi.org/10.1016/j.jtbi.2024.111732>.
12. H. K. Rad, H. Salarieh, A. Alasty, and R. Vatankhah, “Boundary Control of Flexible Satellite Vibration in Planar Motion,” *Journal of Sound and Vibration* 432 (2018): 549–568, <https://doi.org/10.1016/j.jsv.2018.06.052>.
13. W. H. Zhu, *Virtual Decomposition Control*, vol. 60 (Springer Berlin Heidelberg, 2010), <https://doi.org/10.1007/978-3-642-10724-5>.
14. T. D. Nguyen and O. Egeland, “Infinite Dimensional Observer for a Flexible Robot Arm With a Tip Load,” *Asian Journal of Control* 10, no. 4 (2008): 456–461, <https://doi.org/10.1002/asjc.45>.
15. H. Yang, J. Liu, and X. Lan, “Observer Design for a Flexible-Link Manipulator With PDE Model,” *Journal of Sound and Vibration* 341 (2015): 237–245, <https://doi.org/10.1016/j.jsv.2014.12.033>.
16. Y. Liu, X. Chen, Y. Mei, and Y. Wu, “Observer-Based Boundary Control for an Asymmetric Output-Constrained Flexible Robotic Manipulator,” *SCIENCE CHINA Information Sciences* 65, no. 3 (2022): 139203, <https://doi.org/10.1007/s11432-019-2893-y>.
17. Y. Liu, Y. Fu, W. He, and Q. Hui, “Modeling and Observer-Based Vibration Control of a Flexible Spacecraft With External Disturbances,” *IEEE Transactions on Industrial Electronics* 66, no. 11 (2019): 8648–8658, <https://doi.org/10.1109/TIE.2018.2884172>.
18. S. S. Rao, *Vibration of Continuous Systems* (John Wileys, 2007).
19. L. Tang, M. Gouttefarde, H. Sun, L. Yin, and C. Zhou, “Dynamic Modelling and Vibration Suppression of a Single-Link Flexible Manipulator With Two Cables,” *Mechanism and Machine Theory* 162 (2021): 104347, <https://doi.org/10.1016/j.mechmachtheory.2021.104347>.
20. M. R. Homaeinezhad, F. FotoohiNia, and S. Yaqubi, “Active Predictive Vibration Suppression Algorithm for Structural Stability and Tracking Control of Nonlinear Multivariable Continuum-Mechanics Mobile Systems,” *Optimal Control Applications and Methods* 42, no. 2 (2021): 503–525, <https://doi.org/10.1002/oca.2687>.
21. P. Mäkinen and J. Mattila, *Finite Element-Based Control of a Single-Link Flexible Hydraulic Manipulator*. In: *ASME/BATH 2017 Symposium on Fluid Power and Motion Control* (American Society of Mechanical Engineers, 2017), 2003–2005, <https://doi.org/10.1115/FPMC2017-4264>.
22. T. Meurer, *Control of Higher-Dimensional PDEs* (Springer Berlin Heidelberg, 2013), <https://doi.org/10.1007/978-3-642-30015-8>.
23. S. Yaqubi, M. Dardel, and H. M. Daniali, “Nonlinear Dynamics and Control of Crank-Slider Mechanism With Link Flexibility and Joint Clearance,” *Proceedings of the Institution of Mechanical Engineers, Part C: Journal of Mechanical Engineering Science* 230, no. 5 (2016): 737–755, <https://doi.org/10.1177/0954406215593773>.
24. W. He and S. S. Ge, “Robust Adaptive Boundary Control of a Vibrating String Under Unknown Time-Varying Disturbance,” *IEEE Transactions on Control Systems Technology* 20, no. 1 (2012): 48–58, <https://doi.org/10.1109/TCST.2010.2099230>.
25. A. Benabdelhadi, F. Giri, T. Ahmed-Ali, M. Krstic, H. El Fadil, and F. Z. Chaoui, “Adaptive Observer Design for Wave PDEs With Nonlinear Dynamics and Parameter Uncertainty,” *Automatica* 123 (2021): 109295, <https://doi.org/10.1016/j.automatica.2020.109295>.
26. M. Krstic, A. A. Siranosian, A. Smyshlyaev, and M. Bement, “Backstepping Boundary Controllers and Observers for the Slender Timoshenko Beam: Part II—Stability and Simulations,” in *Proceedings of the 45th IEEE Conference on Decision and Control* (IEEE, 2006), 3938–3943, <https://doi.org/10.1109/CDC.2006.377717>.
27. Z. Han, Z. Liu, W. Kang, and W. He, “Boundary Feedback Control of a Nonhomogeneous Wind Turbine Tower With Exogenous Disturbances,” *IEEE Transactions on Automatic Control* 67, no. 4 (2022): 1952–1959, <https://doi.org/10.1109/TAC.2021.3071021>.
28. X. Zhang, W. Xu, S. S. Nair, and V. S. Chellaboina, “PDE Modeling and Control of a Flexible Two-Link Manipulator,” *IEEE Transactions on Control Systems Technology* 13, no. 2 (2005): 301–312, <https://doi.org/10.1109/TCST.2004.842446>.
29. F. Cao and J. Liu, “An Adaptive Iterative Learning Algorithm for Boundary Control of a Coupled ODE–PDE Two-Link Rigid–Flexible Manipulator,” *Journal of the Franklin Institute* 354, no. 1 (2017): 277–297, <https://doi.org/10.1016/j.jfranklin.2016.10.013>.
30. Z. Zhao, Z. Liu, W. He, K. S. Hong, and H. X. Li, “Boundary Adaptive Fault-Tolerant Control for a Flexible Timoshenko Arm With Backlash-Like Hysteresis,” *Automatica* 130 (2021): 109690, <https://doi.org/10.1016/j.automatica.2021.109690>.
31. W. He, X. He, M. Zou, and H. Li, “PDE Model-Based Boundary Control Design for a Flexible Robotic Manipulator With Input Backlash,” *IEEE Transactions on Control Systems Technology* 27, no. 2 (2019): 790–797, <https://doi.org/10.1109/TCST.2017.2780055>.
32. X. He, W. He, H. Qin, and C. Sun, “Boundary Vibration Control for a Flexible Timoshenko Robotic Manipulator,” *IET Control Theory and Applications* 12, no. 7 (2018): 875–882, <https://doi.org/10.1049/iet-cta.2017.1017>.
33. J. Wang, J. Liu, B. Ji, Y. He, S. Xia, and Y. Zhou, “Vibration Suppression and Boundary Control for Nonlinear Flexible Rotating Manipulator in Three-Dimensional Space Subject to Output Restrictions,”

- Communications in Nonlinear Science and Numerical Simulation* 120 (2023): 107151, <https://doi.org/10.1016/j.cnsns.2023.107151>.
34. L. Li and J. Liu, "Nussbaum Function-Based Adaptive Boundary Control for Flexible Manipulator With Unknown Control Directions and Nonlinear Time-Varying Actuator Faults," *International Journal of Robust and Nonlinear Control* 33, no. 12 (2023): 6778–6798, <https://doi.org/10.1002/rnc.6723>.
35. H. Wang, X. Zhou, and Y. Tian, "Robust Adaptive Fault-Tolerant Control Using RBF-Based Neural Network for a Rigid-Flexible Robotic System With Unknown Control Direction," *International Journal of Robust and Nonlinear Control* 32, no. 3 (2022): 1272–1302, <https://doi.org/10.1002/rnc.5880>.
36. T. Jiang, J. Liu, and W. He, "Boundary Control for a Flexible Manipulator With a Robust State Observer," *Journal of Vibration and Control* 24, no. 2 (2016): 260–271, <https://doi.org/10.1177/1077546316635343>.
37. L. Zhang and J. Liu, "Observer-Based Partial Differential Equation Boundary Control for a Flexible Two-Link Manipulator in Task Space," *IET Control Theory and Applications* 6, no. 13 (2012): 2120–2133, <https://doi.org/10.1049/iet-cta.2011.0545>.
38. T. Jiang, J. Liu, and W. He, "Boundary Control for a Flexible Manipulator Based on Infinite Dimensional Disturbance Observer," *Journal of Sound and Vibration* 348 (2015): 1–14, <https://doi.org/10.1016/j.jsv.2015.02.044>.
39. N. Boonkumkrong, S. Chinvorarat, and P. Asadamongkon, "Passivity-Based Boundary Control With the Backstepping Observer for the Vibration Suppression of the Flexible Beam," *Heliyon* 9, no. 1 (2023): e12740, <https://doi.org/10.1016/j.heliyon.2022.e12740>.
40. Q. Xu, Z. Jing, and S. Hu, "Stability Analysis of Nonlinear Dynamic System With Linear Observer for a Multilink Flexible Manipulator," *International Journal of Non-Linear Mechanics* 103 (2018): 27–36, <https://doi.org/10.1016/j.ijnonlinmec.2018.04.007>.
41. N. G. Chalhoub, G. A. Kfoury, and B. A. Bazzi, "Design of Robust Controllers and a Nonlinear Observer for the Control of a Single-Link Flexible Robotic Manipulator," *Journal of Sound and Vibration* 291, no. 1–2 (2006): 437–461, <https://doi.org/10.1016/j.jsv.2005.06.019>.
42. Q. Yao, Q. Li, J. Huang, and H. Jahanshahi, "PDE-Based Prescribed Performance Adaptive Attitude and Vibration Control of Flexible Spacecraft," *Aerospace Science and Technology* 141 (2023): 108504, <https://doi.org/10.1016/j.ast.2023.108504>.
43. W. He, S. S. Ge, B. V. E. How, Y. S. Choo, and K. S. Hong, "Robust Adaptive Boundary Control of a Flexible Marine Riser With Vessel Dynamics," *Automatica* 47, no. 4 (2011): 722–732, <https://doi.org/10.1016/j.automatica.2011.01.064>.
44. M. S. De Queiroz, D. M. Dawson, M. Agarwal, and F. Zhang, "Adaptive Nonlinear Boundary Control of a Flexible Link Robot Arm," *IEEE Transactions on Robotics and Automation* 15, no. 4 (1999): 779–787, <https://doi.org/10.1109/70.782034>.
45. Y. Liu, Y. Mei, H. Cai, C. He, T. Liu, and G. Hu, "Asymmetric Input-Output Constraint Control of a Flexible Variable-Length Rotary Crane Arm," *IEEE Transactions on Cybernetics* 52, no. 10 (2022): 10582–10591, <https://doi.org/10.1109/TCYB.2021.3055151>.
46. Y. Liu, W. Zhan, M. Xing, Y. Wu, R. Xu, and X. Wu, "Boundary Control of a Rotating and Length-Varying Flexible Robotic Manipulator System," *IEEE Transactions on Systems, Man, and Cybernetics: Systems* 52, no. 1 (2022): 377–386, <https://doi.org/10.1109/TSMC.2020.2999485>.
47. W. An, J. Xu, M. Wu, and P. Jiang, "A Method of Deflection of the Vertical Measurement Based on Phase Correction," *IEEE Access* 9 (2021): 5933–5942, <https://doi.org/10.1109/ACCESS.2020.3047392>.
48. H. Zwart, "Sufficient Conditions for Pre-Compactness of State Trajectories," in *IFAC-PapersOnLine*. 53 (Elsevier B.V., 2020), 5298–5302, <https://doi.org/10.1016/j.ifacol.2020.12.1212>.
49. Z. Shi, C. Deng, S. Zhang, Y. Xie, H. Cui, and Y. Hao, "Hyperbolic Tangent Function-Based Finite-Time Sliding Mode Control for Spacecraft Rendezvous Maneuver Without Chattering," *IEEE Access* 8 (2020): 60838–60849, <https://doi.org/10.1109/ACCESS.2020.2983316>.
50. Y. Liu, X. Chen, Y. Wu, H. Cai, and H. Yokoi, "Adaptive Neural Network Control of a Flexible Spacecraft Subject to Input Nonlinearity and Asymmetric Output Constraint," *IEEE Transactions on Neural Networks and Learning Systems* 33, no. 11 (2022): 6226–6234, <https://doi.org/10.1109/TNNLS.2021.3072907>.
51. M. R. Homaeinezhad and S. Yaqubi, "Discrete-Time Sliding-Surface Based Control of Parametrically Uncertain Nonlinear Systems With Unknown Time-Delay and Inaccessible Switching Mode Detection," *International Journal of Control* 94, no. 3 (2019): 1–20, <https://doi.org/10.1080/00207179.2019.1605205>.
52. S. Yaqubi and M. R. Homaeinezhad, "Analytical Single-Mode Sliding Predictive Control of Arbitrarily Switched Nonlinear Systems Incorporating Dynamical Variations," *Nonlinear Analysis: Hybrid Systems* 38 (2020): 100937, <https://doi.org/10.1016/j.nahs.2020.100937>.